12-2018

Thermal Management of Satellite Electronics via Gallium Phase Change Heat Sink Devices

Brian O. Palmer

THERMAL MANAGEMENT OF SATELLITE ELECTRONICS VIA GALLIUM PHASE CHANGE HEAT SINK DEVICES

THESIS

Brian O. Palmer, Major, USAF

AFIT-ENY-MS-18-D-038

DEPARTMENT OF THE AIR FORCE
AIR UNIVERSITY

AIR FORCE INSTITUTE OF TECHNOLOGY

Wright-Patterson Air Force Base, Ohio

AFIT-ENY-MS-18-D-038

THERMAL MANAGEMENT OF SATELLITE ELECTRONICS VIA GALLIUM PHASE CHANGE HEAT SINK DEVICES

THESIS

Presented to the Faculty

Department of Aeronautics and Astronautics

Graduate School of Engineering and Management

Air Force Institute of Technology

Air University

Air Education and Training Command

In Partial Fulfillment of the Requirements for the

Degree of Master of Science in Astronautical Engineering

Brian O. Palmer, BS, MBA

Major, USAF

December 2018

AFIT-ENY-MS-18-D-038

THERMAL MANAGEMENT OF SATELLITE ELECTRONICS VIA GALLIUM PHASE CHANGE HEAT SINK DEVICES

Brian O. Palmer, BS, MBA

Major, USAF

Committee Membership:

Dr. Carl R. Hartsfield, PhD
Chair

Lt Col James L. Rutledge, PhD
Member

Major Ryan P. O'Hara, PhD
Member

Abstract

The purpose of this research was to determine the effectiveness and feasibility of additively manufactured heat sinks using gallium as a phase change material in the thermal management of satellite electronics. A design was created based on the footprint of an Astronautical Development, LLC Lithium 1 UHF radio and six heat sinks were additively manufactured; two each of stainless steel 316, Inconel 718, and ULTEM 9085. Each heat sink was filled with gallium for testing purposes. Models were created to simulate the behavior of the heat transfer and phase change processes occurring within the heat sink. Additionally, laboratory data was gathered on the actual processes occurring. Testing was carried out in a thermal vacuum chamber with the use of film heaters that were attached to the heat sink to simulate a radio in transmitting mode while a satellite is in contact with a ground station. Finally, temperature profiles of the laboratory data were created to gain insight into the characteristics of the phase change process and its effectiveness in thermal management of satellite electronics.

Acknowledgments

I would like to express my sincere appreciation to my faculty advisor, Dr. Carl Hartsfield, for his guidance and support throughout the course of this thesis effort. The insight and experience was certainly appreciated.

Brian O. Palmer

Table of Contents

Page

List of Figures

Page

List of Tables

Page

Nomenclature

A	area, m^2
A_{rad}	radiator area
Bi	Biot number
c	specific heat, J/kg-K
$\dot{E}_{in}$	rate of energy flow in, W
$\dot{E}_{out}$	rate of energy flow out, W
$\dot{E}_{st}$	rate of energy stored, W
h	convection heat transfer coefficient, W/m^2-K
h_r	radiation heat transfer coefficient, W/m^2-K
k	thermal conductivity, W/m-K
L	length, m
L_c	characteristic length, m
q_{cond}	heat transfer rate due to conduction, W
q_{conv}	heat transfer rate due to convection, W
q_{in}	heat flow in, W
q_{rad}	heat transfer rate due to radiation, W
q''	heat flux, W/m^2
R_{cond}	thermal resistance for conduction, K/W
T	surface temperature, K

T_1	temperature at point 1
T_2	temperature at point 2
T_∞	ambient temperature
T_{sur}	temperature of the surroundings
T_i^n	temperature at node (n,i)
x	distance, m
α	thermal diffusivity, m^2/s
Δt	change in time, s
Δx	change in length, m
ε	emissivity
ρ	density, kg/m^3
σ	Stephan-Boltzmann constant, $W/m^2\text{-}K^4$

THERMAL MANAGEMENT OF SATELLITE ELECTRONICS VIA PHASE CHANGE HEAT SINK DEVICES

I. Introduction

1.1 General Issue

The advent of space exploration was a significant event for the world that brought about momentous advances in technology. Modern space vehicles are incredibly complex and expensive machines. Because of this, a significant number of resources are needed to ensure proper design and construction such that the space vehicle operates reliably. Furthermore, performing maintenance on vehicles while in orbit is usually impractical for most systems. This reinforces the idea that reliability is paramount.

Because each space mission is unique, space vehicles are designed around the mission they are to carry out. Of the many problems that must be solved in designing a space vehicle, thermal management of the vehicle's electronics is a critical issue. Heat generated within the space craft can create a detrimental environment to the onboard electronics which may lead to diminished operation [1]. Thus, a means for heat removal is typically required in a space vehicle. One method of passive thermal management involves the use of heat sinks filled with a phase change material, or PCM. A PCM device takes advantage of the latent heat of fusion of a substance where the temperature will remain constant during the transition from solid to liquid even though heat is still being added [2].

1.2 Problem Statement

Excessive heat generated by electronic devices within a space vehicle must be controlled to ensure nominal device operation. Heat sinks containing a PCM offer a method to control excessive heat. Thermal management of satellite electronics using additively manufactured heat sinks with gallium as a PCM needs to be researched to determine the effectiveness of such devices. Also, determining a feasible process for designing and building them to fit a particular application is needed.

1.3 Research Objectives/Questions/Hypotheses

By taking advantage of the phase change phenomenon and gallium's low melting point, satellite electronics can have an effective means of managing waste heat.
The objectives for this research are to 1) determine the effectiveness of gallium PCM heat sinks for satellites with transient electronics operation and 2) devise a process for the design and fabrication of gallium PCM heat sinks using additive manufacturing. This research will provide the necessary insight into the characteristics of phase change heat sinks.

1.4 Methodology, Assumptions, and Equipment

The space environment can be simulated to a reasonable degree in a thermal vacuum chamber. For the purposes of this research, it can create a close representative environment that a space vehicle will encounter in orbit. The vacuum created in the chamber is important since it eliminates convection heat transfer; thermal radiation is the only means of eliminating waste heat in the absence of an atmosphere.

Radios are standard electronic devices found in all space vehicles since they enable communications between the ground stations and the vehicle itself. In this research, radios are replaced with film heaters in order emulate the waste heat that typical radios produce. Thermocouples were used to collect temperature data of the heaters and PCM.

The product of this research is a detailed process of designing and building a heat sink for a particular application. Certain mission parameters will determine the specifications of the heat sink to be created. Since a plethora of space vehicle applications exist, the scope must be narrowed to help facilitate the research. The shape and size of the orbit and location of the ground station will determine the contact time between the satellite and ground station, which will also be the amount of time the radio is transmitting to the ground station. Since the contact time varies over successive orbits, the longest possible contact time will determine the size of the heat sink so that the phase change can be fully utilized. Additionally, the contact time indirectly determines the time available to radiate the waste heat into space.

Testing the heat sink device requires simulating the conditions it will experience in a satellite. The scenario is one of a satellite passing over a ground station, where a pass lasts several minutes. The radio initiates transmission at the beginning of the pass and continues to transmit until the pass is complete, all the while generating heat that is being dumped into the heat sink device. Once the radio has stopped transmitting, the heat sink will radiate this waste heat for the remainder of the simulated orbit until the next pass occurs. The experiment will generate empirical data showing the behavior of the

phase from solid to liquid during radio transmission and then from liquid to solid once transmission has ceased as the heat is radiated away.

In addition to the aforementioned tests, the compatibility of various metals used with gallium was researched. A variety of metals are available for additive manufacturing, but they must be resistant to gallium attack. Gallium's tendency to amalgamate with certain metals (e.g. aluminum) is detrimental in this application and can cause embrittlement of the material; thus, selection of one of these metals would result in premature component failure [3]. Thus, care must be taken when considering a material for the heat sink.

1.5 Preview

This chapter has put forth the objectives and motivation for this thesis. Chapter 2 presents the history and current uses of phase change materials and additive manufacturing. Chapter 3 explains the methodology used in designing the process of building heat sinks as well as the modeling and testing involved. Chapter 4 describes the results and analysis of the experiments performed in this research. Finally, the conclusions, potential applications, and recommendations for future research is presented in Chapter 5.

II. Literature Review

2.1 Chapter Overview

The purpose of this chapter is to present the operation of PCM heat sinks as well as the history and current applications in thermal management. Furthermore, the different types of PCMs that have seen use are explored and the advantages and disadvantages of the various types are presented. This chapter will conclude with a discussion on why gallium as a PCM is beneficial for the thermal management of space vehicle electronics with transient operation. The scenario of a space vehicle in low earth orbit (LEO) is presented to support this concept.

2.2 Heat Sink Operation

At a basic level, a PCM heat sink consists of a shell that encapsulates a PCM (Figure 1). A heat source is in contact with, and transfers heat into, one side of the heat sink. Heat is transferred into the shell, which then passes into the PCM. The PCM will increase in temperature until the melting point is reached. At that point, the material will remain at a fairly constant temperature as heat is being added until enough heat has been added to entirely change the phase from solid to liquid. Heat will pass through the PCM, through the heat sink wall, and finally conducted into a radiator to be expelled into space. This passive form of thermal management is a simple and effective process in a cyclical heat environment.

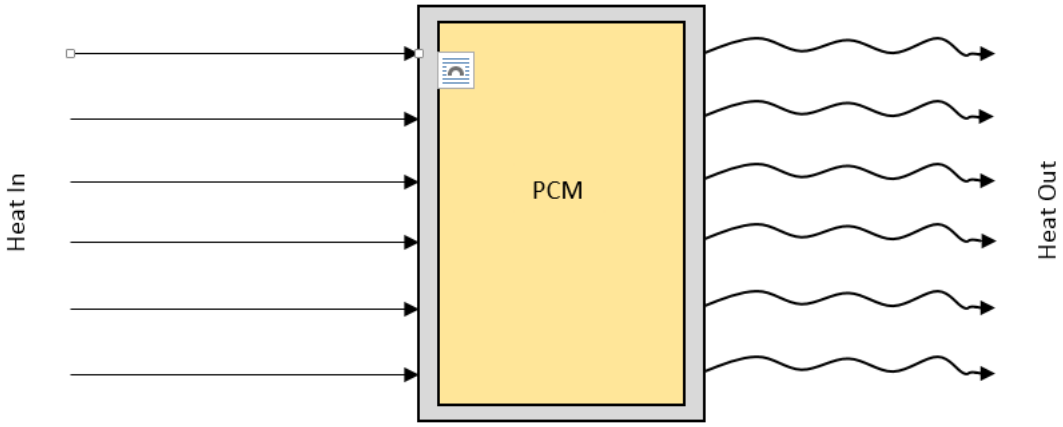

Figure 1 PCM Heat Sink

The amount of time that the PCM can remain at a constant temperature is proportional to the volume of PCM that is present in the heat sink. The latent heat of fusion (or enthalpy of fusion) for a material is the amount of energy required to be added into the system to change the phase from solid to liquid, or alternatively, the amount of energy required to be released to change phase from liquid to solid [4]. Typically, the latent heat of fusion is measured in kilojoules per kilogram $\left(\frac{kJ}{kg}\right)$ or kilojoules per mole $\left(\frac{kJ}{m}\right)$.

Limitations do exist in how effective a PCM thermal device is at managing excessive heat. For instance, PCMs with low thermal conductivities (i.e. insulators) or excessive thicknesses may prevent adequate heat transfer through the medium, which will prevent a constant temperature throughout during phase change. Three regions exist within the PCM during the phase change process: a liquid region, a solid region, and a phase change front between these two. Initially, the entire volume of the PCM is solid. Once melting begins, the liquid region forms and will gradually expand over time

replacing the solid region. As the liquid region expands, the temperature difference across this expanding region will increase out of necessity. For a given linear distance, the thermal conductivity and temperature gradient are inversely proportional. PCMs with very high thermal conductivities will have small temperature gradients across the linear distance, making the PCM to appear isothermal throughout. However, small thermal conductivities will result in large temperature gradients across this distance. Eq 1 below describes the relationship between the thermal conductivity (q_{cond}), the temperature gradient, and the linear distance for heat conduction in the PCM [5]:

$$q_{cond} = kA\frac{dT}{dx} \text{ (Watts)} \qquad \text{Eq 1}$$

where k is the thermal conductivity (W/m-K), A is area (m^2), and $\frac{dT}{dx}$ is the change in temperature (K) with respect to the change in linear distance (m).

2.3 Advantages of PCM Heat Sinks

PCM heat sinks are simple devices that can control temperature simply by taking advantage of the phase change phenomenon. The reliability of a space vehicle is inversely proportional to the number and complexity of the machines onboard, as well as associated power requirements to run them [6]. PCM heat sinks provide a means of achieving this reliability in that they neither require power nor moving parts to function. In comparison to a non-PCM heat sink, a PCM heat sink will maintain a constant temperature during the phase change, essentially creating a delay in temperature increase. The heat that is transferred into the PCM is simply stored during the melting process until

the electronics power down, at which point the accumulated heat is released into the environment as the PCM transitions back to the solid phase. A non-PCM heat sink will continually increase in temperature while heat is being transferred into it, as can be seen in Figure 2 [7]. Chen, et al. showed that a transmitter without a PCM heat sink will increase continually while one with a PCM heat sink will maintain a lower temperature during transmitter operation.

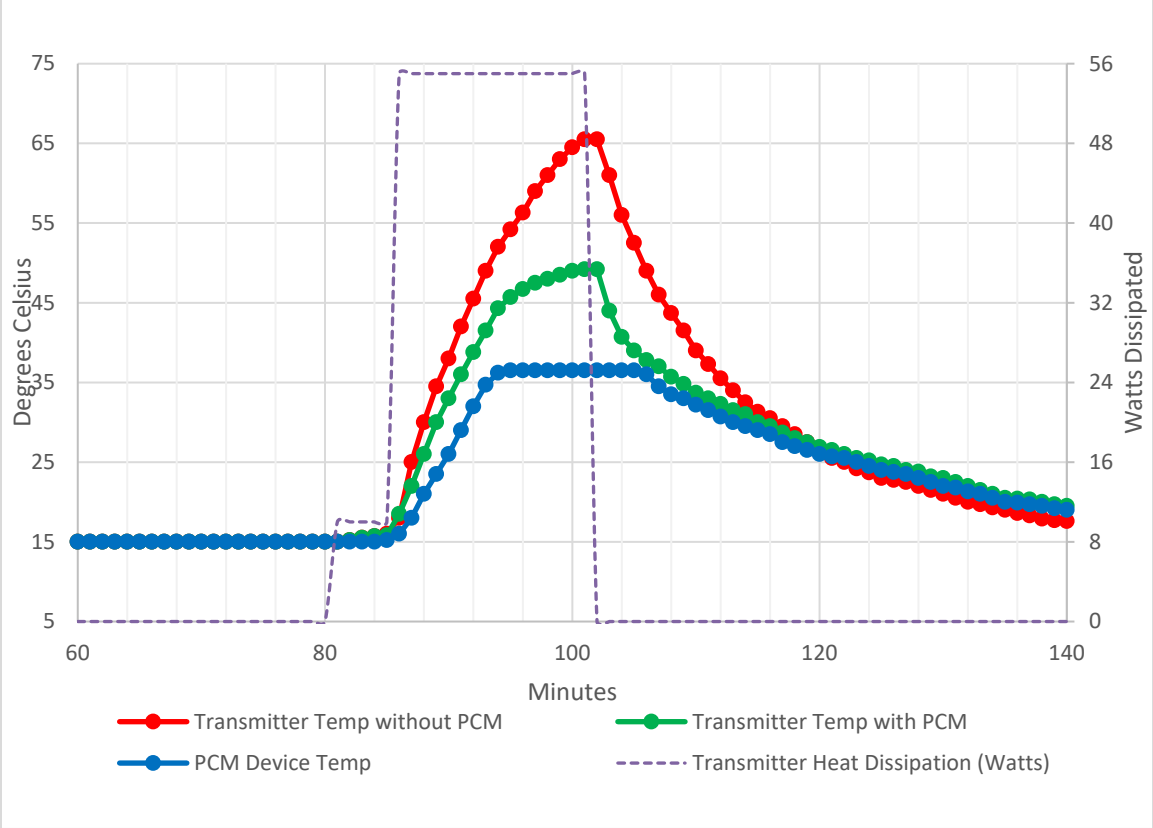

Figure 2 PCM and non-PCM heat sink comparison, based on data from Chen, et. al [7]

2.4 History of PCM Devices

The use of phase change materials in thermal management is not a new concept. NASA has utilized various PCMs throughout its history. The Lunar Roving Vehicles (LRV) used during the Apollo missions, as well as Skylab, used various PCM systems for thermal management [8, 9]. In 2016, the Phase Change Heat Exchanger Project was launched to the International Space Station to study the various applications of a PCM heat exchanger [9]. The MESSENGER space craft, launched in 2004 to study the planet Mercury, utilized PCM packs to regulate the heat of its imaging system [10]. PCMs are even being incorporated into textiles for thermal comfort [11]. A well known utilization of phase change is the ice in a cooler, where the low temperature is maintained for the duration of the melting process. Without this phase change process, the temperature would increase at a steady rate instead of remaining constant.

2.5 Organic and Inorganic Phase Change Materials

A plethora of materials are available that have been researched and utilized for PCM applications. Organic PCMs consist of those materials that contain carbon, such as paraffin, while inorganic PCMs do not [12]. Typically, inorganic PCMs consist of a type of salt, such as sodium sulfate decahydrate ($Na_2SO_410H_2O$). Both types of PCMs tend to offer high values for the latent heat of fusion and a wide range of melting temperatures is available depending on the application.

Table 1 shows several phase change materials and their various properties that are commercially available from PCM Products, Limited [13].

Table 1 Commercially Available PCMs [13]

PCM Type	PCM	Melting Temp (K)	Density (g/mL)	Latent Heat (J/g)	Latent Heat (J/mL)	Specific Heat Capacity (J/g-K)	Thermal Conductivity (W/m-K)
Hydrated Salts	S32	305	1.46	200	292	1.91	0.51
	S30	303	1.304	190	247.76	1.9	0.48
	S27	300	1.53	183	279.99	2.2	0.54
Organics	A32	305	0.845	130	109.85	2.2	0.21
	A29	302	0.81	226	183.06	2.15	0.18
	A28	301	0.789	155	122.30	2.22	0.21
	A26	299	0.79	150	118.50	2.22	0.21

However, most PCMs have low thermal conductivities, typical of materials used for thermal insulation [14]. This can become problematic in PCM heat sinks since low thermal conductivity can also be associated with low thermal diffusivity where a material is slow to conduct and release heat. A way to mitigate this is to build a heat sink with thermal conductivity enhancers.

2.6 Thermal Conductivity Enhancers

The internal configuration of the heat sink will affect how heat is transferred into the PCM. The greater the surface area of the heat sink that is in contact with the PCM, the larger the heat transfer will be. One method of increasing the surface area is to utilize a thermal conductivity enhancer (TCE). A TCE is simply material with a high thermal conductivity that protrudes from the wall of the heat sink into the PCM.

One type of TCE is the pin fin. Chen, Huang, and Chen tested three PCM heat sinks with different internal configurations, each filled with n-eicosane [7]. Two heat sinks had similar pin-finned configurations to each other, while a third heat sink had no fins. Each of the three configurations had a unique temperature profile.

The experiments showed a more effective heat transfer from the heat sink wall into the PCM with the finned configurations compared to the non-finned configuration. The fins helped to bring heat deep into the PCM where it was heated almost in an inside-out manner, in addition to being heated by the heat sink walls. The opposite was true for the non-finned configuration. In this case, the PCM could only be heated from the outside-in. Additionally, the finned heat sinks transferred more heat into PCM than the non-finned heat sink during the time span that the heat source was operating [7].

Saha, Srinivasan, and Dutta also researched the use of pin-fins as well as plate-fins as TCEs. Additionally, they researched the optimal configuration of fins dispersed within the PCM [14]. In their research, they investigated the TCE to PCM volume ratios within the heat sink to determine an optimum value. Assuming a heat sink occupies a fixed volume, increasing the TCE volume within the sink will inherently decrease the PCM volume. While a greater TCE volume will transfer heat more effectively in the PCM, this naturally leaves less PCM to absorb energy during melting. Additionally, the performance of pin-fins to that of plate-fins was studied. Surface area is an important factor in heat transfer, with an increasing surface area resulting in increased heat transfer. The same volumetric ratio could be attained for the two types of fins, but the pin-fins resulted in an increased surface area for the given volumetric ratio. For the heat sink

configuration in their experiment, it was concluded that a TCE to PCM ratio of 8% yielded the most effective results with the use of pin-fins [14].

Since most PCMs have low thermal conductivities [14], the use of fins may be necessary in order to conduct heat into the PCM in a timely manner. Also, fins may be necessary based on the conditions the heat sink may encounter. If the low thermal conductivities of traditional PCMs are undesirable for an application, metallic PCMs might offer a reasonable alternative.

2.7 Metallic Phase Change Materials

A small number of pure elemental metals exist in the liquid phase near room temperature. Among these are gallium, caesium, rubidium, and mercury [15]. Of the four metals, gallium, caesium, and rubidium have similar melting points, with mercury's melting point being much lower. Table 2 below shows properties of the four unalloyed elements.

Table 2 Comparison of Low Melting Point Metals (Solid Phase) [15]

Element	Melting point (K)	Density (g/mL)	Latent heat of fusion (per mass) (J/g)	Latent heat of fusion (per volume) (J/mL)	Specific Heat Capacity (J/g-K)	Thermal conductivity (W/m-K)
Gallium	302.8	5.91	80.12	473.27	0.37	29.4
Caesium	301.7	1.80	16.4	29.45	0.236	17.4
Rubidium	311.9	1.47	25.74	37.83	0.363	29.3
Mercury	234.1	13.55	11.4	154.42	0.139	8.34

From Table 2, gallium's latent heat of fusion is higher than the other three metals enabling it to absorb much more energy during a phase change. From a mass perspective, gallium can absorb about three to seven times more heat per gram than the

other metals. From a volume perspective, the element can absorb about three to 16 times the energy per milliliter, making gallium the obvious choice as a metallic phase change material. It's worth noting that the density of an element plays a role in the overall amount of heat that can be absorbed for a given volume. Density multiplied by the latent heat (per mass) yields the latent heat per volume. Thus, a higher density will have a greater impact on the overall available latent heat. From a mass perspective, mercury has the lowest latent heat of fusion of the four metals shown in Table 2, but has the second highest value from a volume perspective. However, given its low melting point, applications as PCMs for thermal management in space vehicle electronics are unlikely. In addition to these 4 metals, several others exist, as well as a collection of alloys with melting temperatures ranging from 47 °C to over 270 °C with potential PCM applications [15].

Ge and Liu compared PCM heat sinks with a variety of PCMs, including gallium, for the thermal management of smartphones [16]. Similar to satellite electronics with transient operation, smartphones also tend to have transient operation (e.g. telephone calls or data transmission). Several trials were conducted that compared equal volumes of sodium sulfate decahydrate, paraffin, n-eicosane, and gallium. Each material was filled in a stainless steel container to form a PCM heat sink used in testing [16]. Heaters were applied to the heat sink to simulate the heat source inside a smartphone. The container's temperature profiles with each PCM were compared and the results demonstrated the effectiveness of gallium for thermal management, as can be seen in Figure 3.

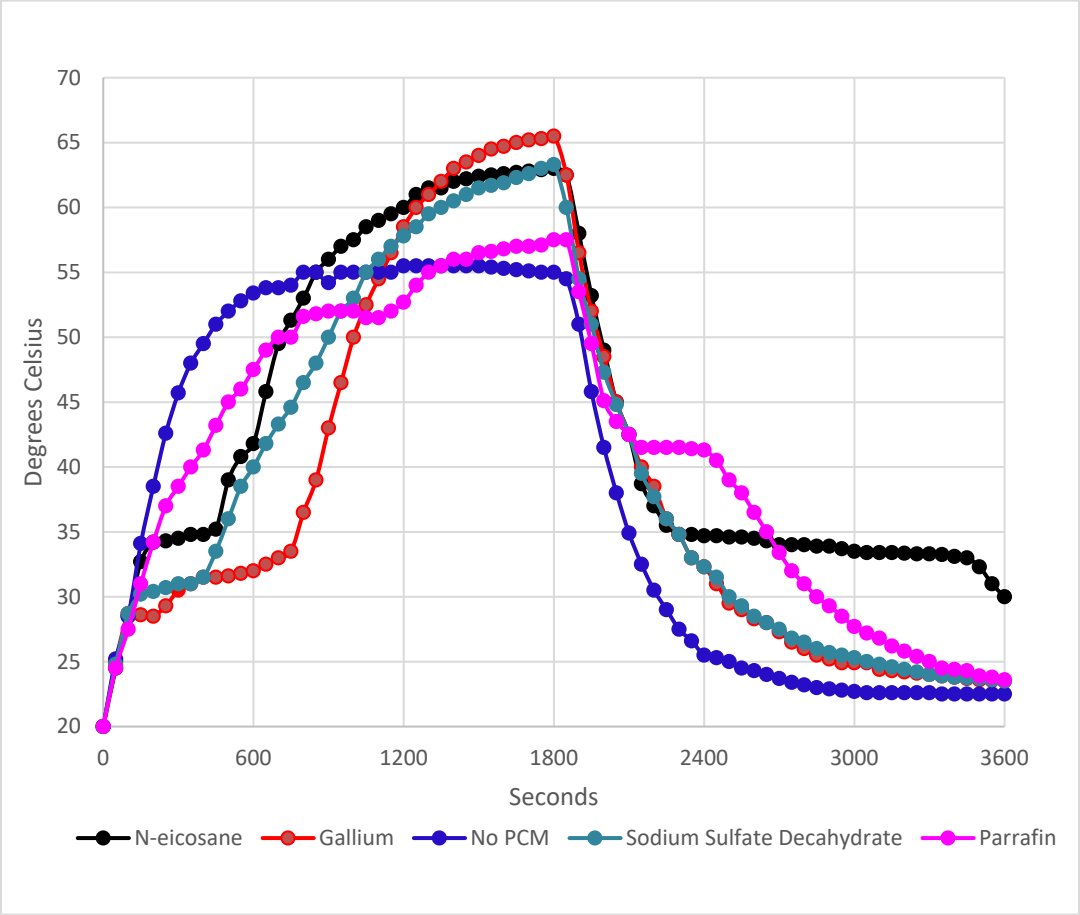

Figure 3 Test trials of multiple PCMs, based on data from Ge, et al [16]

Compared to the other PCMs, gallium had the longest phase change duration. Subsequently, gallium maintained a relatively constant temperature much longer than the trials that used other PCMs. Given the limitation of space within mobile devices, PCM heat sinks offer a reasonable method to manage heat while at the same time maintaining the slim profile that is characteristic of modern devices.

2.8 Gallium Peculiarities

One of gallium's peculiar traits is its tendency to supercool (i.e. remain in the liquid phase at a temperature below its melting point, not to be confused with freezing point depression) [7, 16]. Supercooling is typically undesirable in a PCM heat sink because a supercooled material still retains the latent heat of fusion. If, at the end of a cycle, the material becomes supercooled, the beginning of the next cycle will not be able to take advantage of the phase change process if the material has not begun to solidify. As such, the heat sink will increase in temperature as heat is applied and will continue to rise as the temperature approaches and passes gallium's melting point without holding constant.

Certain methods exist to mitigate gallium's supercooling tendency. Adding impurities to gallium is one option [7, 15]. By doing so, the impurities assist in creating a crystalline structure that will promote freezing of the gallium. Another method is to shake the gallium to encourage nucleation [16]. However, in a space vehicle in orbit, shaking is not a viable option. A reasonable method to prevent supercooling is to ensure the heat sink is designed so that it holds a certain percentage more PCM than is necessary for the scenario [7]. Supercooling is greatly reduced if liquid gallium is in contact with solid gallium. Assuming the maximum contact time is 10 minutes, having enough gallium to last for 11 or 12 minutes will ensure that the gallium never entirely changes phase from solid to liquid. However, being in a spacecraft, this presents a concern over excessive mass and volume.

A second peculiarity of gallium is its innate ability to readily form alloys with most metals, even at low temperatures [3]. Because of this, the material out of which the heat sink is constructed must be considered. Aluminum is a prime example of a metal that readily reacts with gallium. As aluminum becomes soft and brittle after contact with gallium, it cannot be considered as a heat sink material. Stainless steel, as demonstrated in Ge's and Liu's research, is one metal that is resistant to gallium attack [16]. In addition to material compatibility with gallium, the material's thermal conductivity should also be considered. The shell of the heat sink must transfer heat into and out of the PCM quickly enough for this to be a viable option for thermal management. The higher the thermal conductivity, the better the heat transfer.

A third peculiarity of gallium occurs when it changes phase from liquid to solid, gallium will expand by about 3% upon freezing [3]. This must be considered in the heat sink design. When considering the amount of gallium for a heat sink, the calculations are based on the mass of the material. The volume of gallium inside the heat sink is derived using the density. However, since gallium expands upon freezing, the densities for solid and liquid will be different. The volume of solid gallium must be used in the design to ensure the expanding gallium does not exceed the available volume of the heat sink.

2.9 Additive Manufacturing

A stipulation of this research was that additive manufacturing must be utilized in designing and building a gallium-containing heat sink device. Additive manufacturing, also known as rapid prototyping or 3-D printing, is a form of manufacturing in which an object is created by adding layer upon layer in a successive fashion to form a finished

product, typical from a three-dimensional model built using computer aided design (CAD) software [17, 18]. This process offers the ability to create complex shapes that are difficult or impossible to build with traditional manufacturing techniques. Two methods of additive manufacturing that were used in this research include Direct Metal Laser Sintering (DMLS) and Fused Deposition Modeling (FDM) processes.

DMLS is a process that uses a powder bed system in assembling an object [19]. In a powder bed system, a layer of metal powder is spread across a platform and an energy source (e.g. laser), applies heat to melt the metal powder at specified locations according to the CAD file. Once a layer is complete, the platform holding the powder bed is lowered a small distance and another layer of metal powder is added, followed again by the energy source melting powder at specified locations. This process is continued until layer by layer until the desired part is finalized. FDM uses a different approach. The FDM process, created by the company Stratasys, uses a polymer filament that is melted and extruded from a nozzle within the build chamber, tracing and filling the shape of each successive layer of the printed part [18].

2.10 Heat Transfer

2.10.1 Steady State

Heat can be transferred by three different methods: conduction, convection, and radiation. Under steady state conditions, the heat flowing through an object is constant. In other words, heat flowing in is equal to heat flowing out. The three methods can be expressed by the following equations for steady-state conditions where the temperature does not change with respect to time [5]. The equation for conduction is:

$$q_{cond} = \frac{kA}{x}(T_1 - T_2) \text{ (Watts)} \quad \text{Eq 2}$$

Where q_{cond} *is conductive heat transfer, k* is *thermal conductivity* (W/m-K), *A* is *area* (m^2), *x* is *linear distance* (m), and $(T_1 - T_2)$ is *the temperature difference* (Kelvin). Next, heat transfer via convection is expressed as:

$$q_{conv} = hA(T - T_\infty) \text{ (Watts)} \quad \text{Eq 3}$$

where *h* is *heat transfer coefficient*, *T* is *surface temperature*, and T_∞ is *ambient temperature.* Finally, radiative heat transfer is described as:

$$q_{rad} = \epsilon\sigma A_{rad}(T^4 - {T_{sur}}^4) \text{ (Watts)} \quad \text{Eq 4}$$

where ε is *emissivity*, σ is the *Stephan-Boltzmann constant*, A_{rad} is the *radiating area*, *T* is *surface temperature*, and T_{sur} is the *surrounding temperature*. Eq 4 can also be expressed as:

$$q_{rad} = h_r A_{rad}(T - T_{sur}) \quad \text{Eq 5}$$

where

$$h_r = \epsilon\sigma(T^2 + {T_{sur}}^2)(T + T_{sur}) \text{ (W/m}^2\text{K)} \quad \text{Eq 6}$$

2.10.2 Transient Conduction

In instances when heat transfer changes with time, transient conduction within the object exists. Eq 7, the energy balance equation, works as a starting point in the analysis of transient conduction and is useful for deriving equations for boundary conditions.

$$\dot{E}_{in} - \dot{E}_{out} = \dot{E}_{st} \quad \text{Eq 7}$$

The heat equation for one dimensional conductive heat transfer is a parabolic partial differential equation and is expressed as [20]:

$$\frac{\partial T}{\partial t} = \alpha \frac{\partial^2 T}{\partial x^2} \quad \text{Eq 8}$$

where α is the thermal diffusivity expressed as $\alpha = k/\rho c_p$, where ρ is density and c_p is specific heat.

Differential equations, such as the heat equation, can present a degree of difficulty in solving. Finite differences can be used to approximate these differential equations by transforming them into an algebraic expressions that simplify the process [20]. The finite difference method is a useful tool in modeling the behavior of differential equations, such as the heat equation.

2.10.3 Lumped Capacitance Method

The lumped capacitance method is a simpler way of determining transient conduction within an object when compared to the heat equation. However, it only holds true under certain circumstances. The Biot number, defined as:

$$Bi = \frac{hL_c}{k} \quad \text{Eq 9}$$

where L_c is *volume over surface area,* can be thought of as the ratio of convective thermal resistance between and object and a surrounding fluid to the object's conductive thermal resistance [5]. In order for the lumped capacitance method to be valid, the Biot number must be less than 0.1 [5]. Additionally, if h_r from Eq 6 is substituted for h, the Biot number for a radiating object may be approximated. It should be noted that the Biot number for a radiating object will vary with the object's temperature.

2.11 Summary

This chapter has put forth the operational concept of PCM heat sinks as well as a brief history and current applications of these devices. The various PCMs were compared and analyzed for particular applications. The advantages and disadvantages of gallium as a PCM were presented to reinforce the need for this research. Additive manufacturing and heat transfer have also been discussed to provide a proper background of this research. Further research should be performed in the area of gallium PCM thermal management systems for space vehicle electronics as well as gallium PCM heat sink design for additive manufacturing purposes.

III. Methodology

3.1 Chapter Overview

The purpose of this chapter is to present the methodology that was utilized in characterizing the performance of additively manufactured PCM heat sinks. This study sought to demonstrate the effectiveness and feasibility of designing and manufacturing such devices as well as their performance for passive thermal management of spacecraft electronics.

3.2 Problem Review

The electronic devices built into satellites can generate excessive heat during operation. In many situations, these devices have transient operation where the device will be activated for a few minutes out of the entire orbit, such as radios passing over a ground station. Electronics can become excessively warm during the time they are operational. The only means of getting rid of excessive heat in a satellite is to radiate it out into space. The problem with this method of heat transfer is that the electronics can generate heat faster than the heat is being radiated away, which may result in a significant temperature increase.

The PCM heat sink offers a means of thermal management during transient operation of satellite electronics. The advantage of using PCM heat sinks is that they will maintain a steady temperature when undergoing a phase change while the electronics are producing heat. Once the electronics are powered down, the latent heat that is stored within the PCM is released into space via radiation. Thus, while heat is being produced

faster than it can be radiated away, the PCM within the heat sink will absorb this heat without increasing in temperature until the PCM becomes saturated.

3.3 PCM Heat Sink Design

The AstroDev Lithium 1 UHF radio is a typical radio used in cubesats for communication. Based on the footprint of this radio, a PCM heat sink was designed by the author using SolidWorks 2016. Four were built via the Direct Metal Laser Sintering (DMLS) additive manufacturing process: two of 316 stainless steel produced by i3D MFG™ and two of Inconel 718 produced in-house at AFIT. Additionally, two heat sinks made of ULTEM 9085 were built by Stratasys using the Fused Deposition Modeling (FDM) process. A CAD image of the exterior and interior of the heat sink is shown below in Figure 4.

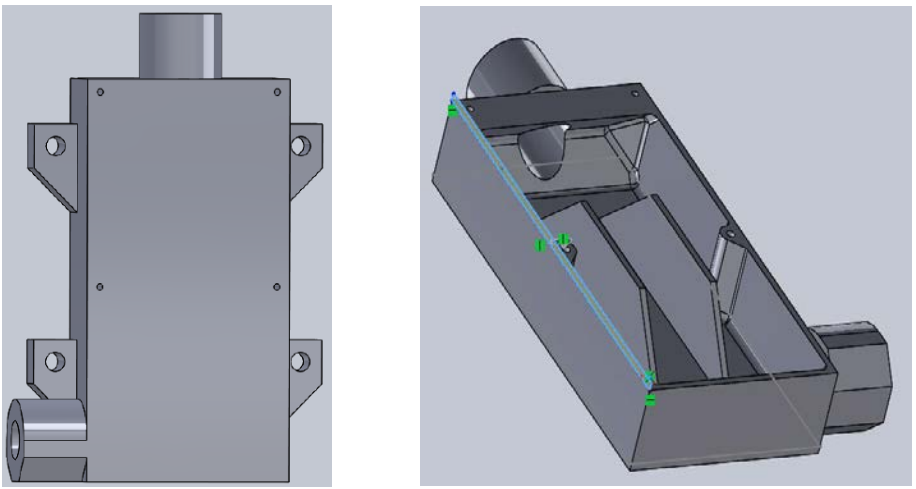

Figure 4 Gallium Heat Sink as designed by the author

This design, as Figure 4 shows, the heat sink has two filling ports, one on top and one at the lower left side. These were incorporated in the design to assist in the removal

of metal powder that remains in the interior of the heat sink during the DMLS process as well as to allow gallium to be poured in and sealed. Additionally, mounting tabs were included to mount the heat sink to the side of a typical cubesat panel, as well as mounting holes for a radio to be attached to the heat sink. These last features were included as a proof of concept in the design and were not utilized during testing. Two thin support structures were included in the design to reinforce the front and rear faces of the heat sink. These structures would also function as TCEs in the situation where the PCM had a lower thermal conductivity than the housing material. However, these do not function as TCEs with gallium as the PCM since its thermal conductivity is much higher than that of the housing material. Each heat sink was designed to hold 100 grams of gallium (16.9 mL solid, 16.4 mL liquid).

Figure 5 below shows a profile of the heat sink with the radiator attached, as well as the resulting composite wall. The composite wall consists of the first heat sink face, the gallium, the second heat sink face, and finally the radiator.

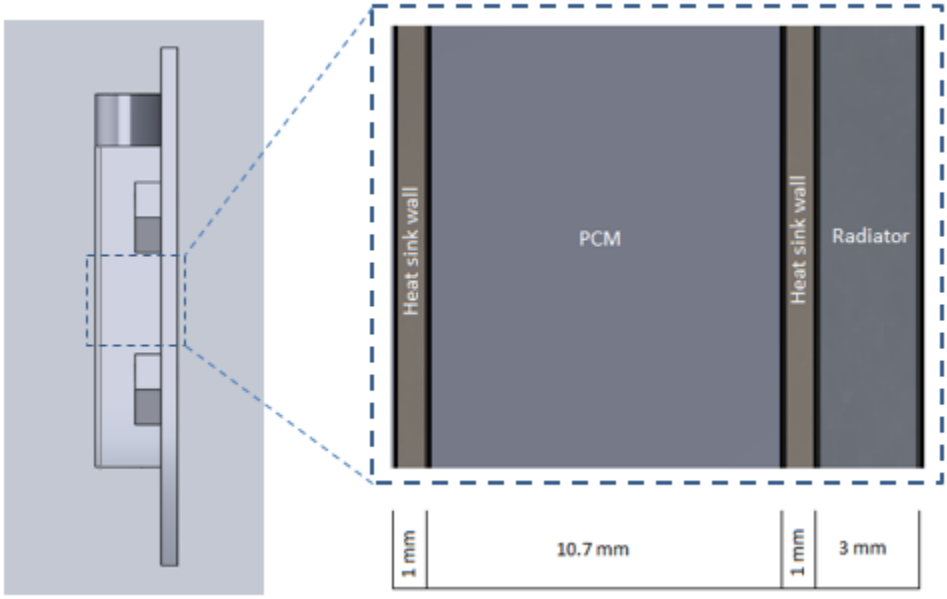

Figure 5 Heat sink and radiator composite wall

3.4 Modeling and Simulation

The operation of the radio is dependent on several factors: the number of ground stations, orbital altitude and inclination, and the antenna apertures. Operating in LEO, a satellite's radio will have an on/off transient operation where it will be on, or transmitting, (and producing waste heat) during a ground pass, and off when not in radio contact with a ground station. The factors mentioned above determine the frequency and duration of radio operation as well as the amount of time between ground passes. Systems Tool Kit, or STK, was used to determine the frequency and duration of contact times between the satellite and the various ground stations.

Heat transfer models were developed in order to demonstrate the behavior of the phase change process. The ground contact data produced from STK showed the transient operation of the radio, which was used in the heat transfer model to simulate the multiple

melting/freezing phase changes that occur over a period of time during an orbit. The MATLAB Code that was generated can be found in Appendix A: MATLAB Code.

3.4.1 Heat Equation Model

For the development of the simulation, the heat equation was modelled using a finite difference method to characterize the behavior of the system. The explicit forward-time, center-space method was used to simulate the transient conduction along the test article as well as the phase change behavior.

Referencing back to Figure 5, heat is applied to the heat sink wall, flowing from left to right in the figure. Heat then flows through the PCM, into the opposite heat sink wall, and finally through the radiator. Eq 8, the heat equation mentioned in chapter 2, is transformed into a finite difference equation by setting the partial derivatives equal to a finite difference between two points as shown in equations 10 and 11.

$$\frac{\partial T}{\partial t} = \alpha \frac{\partial^2 T}{\partial x^2} \qquad \text{Eq 8}$$

$$\frac{\partial T}{\partial t} = \frac{T_i^{n+1} - T_i^n}{\Delta t} \qquad \text{Eq 10}$$

$$\frac{\partial^2 T}{\partial x^2} = \frac{(T_{i+1}^n - 2T_i^n + T_{i-1}^n)}{\Delta x^2} \qquad \text{Eq 11}$$

where n indicates the time node, i indicates the spatial node, Δt is the time difference between nodes and Δx is the spatial difference between nodes. Substituting these expressions into equation 7 yields:

$$\frac{T_i^{n+1} - T_i^n}{\Delta t} = \frac{\alpha}{(\Delta x)^2}(T_{i+1}^n - 2T_i^n + T_{i-1}^n) \quad \text{Eq 12}$$

Rearranging for T_i^{n+1} yields equation 12:

$$T_i^{n+1} = T_i^n + \frac{\alpha \Delta t}{(\Delta x)^2}(T_{i+1}^n - 2T_i^n + T_{i-1}^n) \quad \text{Eq 13}$$

Equation 12 is the expression used to find the temperature at the next time step based on known temperatures at the previous time step. Figure 6 shows a visual depiction of the finite difference grid at a particular point.

T_{i-1}^n	T_i^n	T_{i+1}^n
	T_i^{n+1}	

Figure 6 Finite Difference Grid

The grid used in this simulation had 158 spatial nodes to represent the 15.7 millimeters of thickness of the combined heat sink and radiator with a Δx of 0.0001 meters between nodes. Additionally, the grid had 10001 time nodes with a Δt of 0.0001 seconds to represent one second of simulation time. Overall, the grid used for simulation had a size of 10001 x 158 nodes to model the transient conduction within the heat sink and radiator over the one second time span. The temperature data at the end of each iteration was stored in a separate matrix and the process was repeated until the specified modeling time has been reached.

3.4.1.1 Boundary Conditions

The exterior nodes of the finite difference grid serve as the boundary conditions. For the exterior nodes, the equation must be modified to accommodate *i*-1 and *i*+1 when i

equals 0 (heater node) and 158 (radiator node), respectively. Using the energy balance equation (Eq 7) mentioned previously,

$$\dot{E}_{in} - \dot{E}_{out} = \dot{E}_{st} \qquad \text{Eq 7}$$

and assigning the proper expressions to each $\dot{E}$, an equation can be derived for these nodes. For i = 0, the energy balance equation is expressed as:

$$q"A + \frac{kA}{\Delta x}(T_1^n - T_0^n) = \rho A \frac{1}{2}\Delta x c \frac{dT}{dt} \qquad \text{Eq 14}$$

where $q"A$ is the heat flux times the area, or simply q_{in}. Rearranging to find $\frac{dT}{dt}$ yields:

$$\frac{dT}{dt} = \frac{2\left[q_{in} + \frac{kA}{\Delta x}(T_1^n - T_0^n)\right]}{\rho A \Delta x c} \qquad \text{Eq 15}$$

Substituting the finite difference equation for $\frac{dT}{dt}$ yields:

$$\frac{T_0^{n+1} - T_0^n}{\Delta t} = \frac{2\left[q_{in} + \frac{kA}{\Delta x}(T_1^n - T_0^n)\right]}{\rho A \Delta x c} \qquad \text{Eq 16}$$

Putting in terms of T_0^{n+1} yields:

$$T_0^{n+1} = T_0^n + \frac{2\left[q_{in} + \frac{kA}{\Delta x}(T_1^n - T_0^n)\right]\Delta t}{\rho A \Delta x c} \qquad \text{Eq 17}$$

Equation 17 is the expression used for temperature at i = 0 for all values of n.

In a similar fashion, the equation for the node at i = 158 (the radiator) can be found. To derive the equation for this node, begin with the energy balance equation and assign the proper expression for each $\dot{E}$:

$$\frac{kA}{\Delta x}(T_{i-1}^n - T_i^n) + \epsilon\sigma A\left(T_i^{n\,4} - T_{sur}{}^4\right) = \rho A \Delta x c \frac{dT}{dt} \qquad \text{Eq 18}$$

Putting in terms of $\frac{dT}{dt}$ yields:

$$\frac{dT}{dt} = \frac{\frac{kA}{\Delta x}(T_{i-1}^{n} - T_i^n) + \epsilon\sigma A\left({T_{sur}}^4 - T_i^{n4}\right)}{\rho A \Delta x c} \quad \text{Eq 19}$$

Replacing $\frac{dT}{dt}$ with the finite difference equation results in:

$$\frac{T_i^{n+1} - T_i^n}{\Delta t} = \frac{\frac{kA}{\Delta x}(T_{i-1}^{n} - T_i^n) + \epsilon\sigma A\left({T_{sur}}^4 - T_i^{n4}\right)}{\rho A \Delta x c} \quad \text{Eq 20}$$

Rearranging for T_i^{n+1} , the equation for temperature at i = 158 for all values of n is:

$$T_i^{n+1} = T_i^n + \frac{\left[\frac{kA}{\Delta x}(T_{i-1}^{n} - T_i^n) + \epsilon\sigma A\left({T_{sur}}^4 - T_i^{n4}\right)\right]\Delta t}{\rho A \Delta x c} \quad \text{Eq 21}$$

3.4.1.2 Initial Condition

The AstroDev Li-1 radio has an operating temp of -30 to 70 degrees Celsius [21]. For this scenario, the radio is being held at a constant 0°C, or 273 K, prior to transmitting. The initial temperature distribution for a heat sink made of Stainless Steel 316 is shown in Figure 7. This temperature distribution represents the initial condition for the simulation and, along with the boundary conditions previously specified, is used in solving the heat equation for the model. The distribution represents a composite wall consisting of the heat sink wall, PCM, the second heat sink wall, and the aluminum radiator.

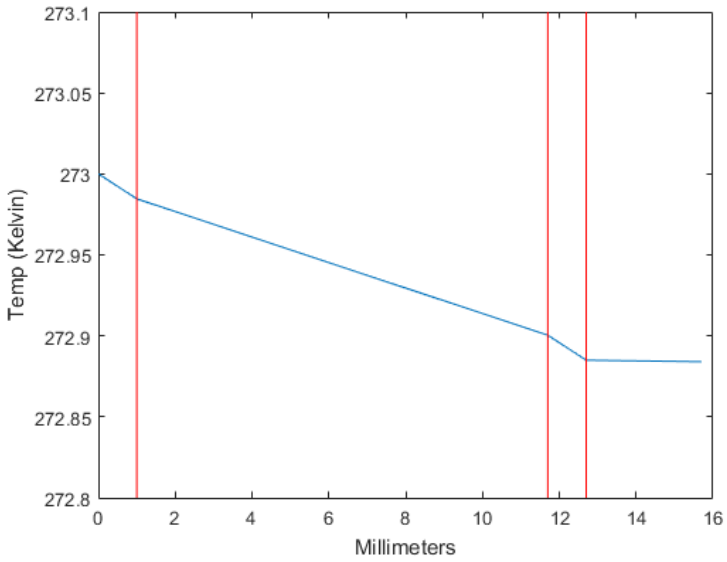

Figure 7 Initial Temperature Distribution

3.4.1.3 Phase Change

The phase change process was modelled by tracking the change in the latent heat of fusion at each time step while the PCM was at the melting temperature. This was accomplished through the use of an array containing nodes that corresponded to the PCM nodes in the temperature grid. Entrance and exit criteria was established in order to begin and end the phase change.

For the melting process, the latent heat at a node was set to zero if the corresponding node in the temperature grid was less than the melting point. As soon as the melting point had been reached at that node, the temperature remained constant while latent heat increased. Latent heat was calculated by measuring the change in energy at that node at every time step until enough energy had accumulated to reach the maximum value of latent heat for that node. At this time, the temperature was again allowed to

increase and the latent heat was held at the maximum value. Figure 8 shows an example of the phase change that is occurring from nodes 24 to 27 of the temperature grid (which corresponds to 2.3 mm to 2.6 mm from the heat source in the assembly).

Spatial Nodes

Time Steps (Seconds)	2.3 mm	2.4 mm	2.5 mm	2.6 mm
	24	25	26	27
807	302.9142	302.9000	302.8962	302.8925
808	302.9142	302.9000	302.8962	302.8925
809	302.9142	302.9000	302.8962	302.8925
810	302.9269	302.9134	302.9000	302.8960
811	302.9284	302.9142	302.9000	302.8962
812	302.9285	302.9142	302.9000	302.8962
813	302.9285	302.9142	302.9000	302.8962
814	302.9285	302.9142	302.9000	302.8962

Figure 8 Temperature Grid (in Kelvin)

Nodes 24 and 25 at the last time step, 814 seconds, are above the melting point (302.9 Kelvin) while node 26 is at the melting point and node 27 is below.

Spatial Nodes

	2.3 mm	2.4 mm	2.5 mm	2.6 mm
	24	25	26	27
1	74.8785	74.8785	24.5659	0

Figure 9 shows the enthalpy array for the nodes corresponding to the temperature matrix at that particular time. For 100 grams of gallium, the maximum latent heat is approximately 74.9 Joules at each node in the PCM. Corresponding with nodes 24 and 25 with the temperature grid, these nodes in the enthalpy array are at the max value while node 26 is less (i.e. still undergoing phase change). Node 27 of the enthalpy array is at

zero which corresponds to the same node on the temperature grid being under the melting point.

	Spatial Nodes			
	2.3 mm	2.4 mm	2.5 mm	2.6 mm
	24	25	26	27
1	74.8785	74.8785	24.5659	0

Figure 9 Enthalpy Array (in Joules)

The solidification process was carried out in reverse fashion as the melting process. While the temperature was above the melting point at a particular node on the temperature grid, the corresponding node in the enthalpy array was at the maximum value. When the temperature decreased to the melting point, the latent heat began to decrease while the temperature remained constant. When the latent heat reached zero, the temperature in the temperature grid resumed decreasing.

3.4.2 Lumped Capacitance Model

A simpler model based on the lumped capacitance method was also developed. The advantage of this model over the previous one is that it requires significantly less computational power to run simulations. Again, starting with the energy balance equation:

$$\dot{E}_{in} - \dot{E}_{out} = \dot{E}_{st} \qquad \mathbf{7}$$

and substituting the equations for energy flow and storage, equation 22 is obtained:

$$\dot{q}_{in} - \epsilon\sigma A_{rad}(T^4 - T_{sur}{}^4) = \rho V c \frac{dT}{dt} \qquad \text{Eq 22}$$

Rearranging in terms of $\frac{dT}{dt}$ yields equation 23:

$$\frac{dT}{dt} = \frac{\dot{q}_{in} - \epsilon\sigma A_{rad}(T^4 - {T_{sur}}^4)}{\rho V c} \quad \text{Eq 23}$$

Since the heat sink and radiator consist of a composite wall of differing materials, the average specific heat for the assembly was calculated based on the sum of percentages of the masses for each component of the wall. The model assumes a uniform temperature throughout the heat sink and radiator and tracks the temperature at a time step of one second over the course of the simulation. The model determines the temperature at the next time step using the previous time step's temperature and Eq 23 (the slope of the curve at the heat sink's current temperature). This is shown in Eq 24:

$$Temp = \frac{dT}{dt} * dt + Previous\ Temp \quad \text{Eq 24}$$

Like the heat equation model, the phase change is modelled by measuring the change in the latent heat of fusion at each time step (Eq 25). Since the temperature is assumed to be constant across the heat sink and radiator at each time step, the simulation of the phase change is simpler. The latent heat is set to zero while the temperature is below the melting point. Once the melting point is reached, the temperature is held constant and the latent heat begins to increase. Once the maximum value for the latent heat is reached (8012 Joules for 100 grams of gallium), the temperature resumes increasing.

$$Latent\ Heat = (\dot{q}_{in} - \dot{q}_{out}) * dt + Previous\ Latent\ Heat \quad \text{Eq 25}$$

The solidification process is again the reverse of this. While the temperature is above the melting point, the latent heat is set at the maximum. Once the temperature has

decreased to the melting point, the temperature is held constant while the latent heat decreases. Once the latent heat reaches zero, the temperature again resumes decreasing.

Figure 10 shows the four-column matrix used for the lumped capacitance model. The first column is the time steps in seconds. The second column calculates the temperature at each time step while the third column calculates the slope of the temperature curve at each time step. The fourth column determines the latent heat of fusion while the temperature is at the melting point.

Time (sec)	Temp (Kelvin)	dT/dt (Kelvin / sec)	Latent Heat (Joules)
525	302.6271	0.0476	0
526	302.6748	0.0476	0
527	302.7224	0.0476	0
528	302.7700	0.0476	0
529	302.8176	0.0476	0
530	302.8651	0.0475	0
531	302.9127	0.0475	0
532	302.9000	0.0475	7.8072
533	302.9000	0.0475	15.6152
534	302.9000	0.0475	23.4232
535	302.9000	0.0475	31.2312
536	302.9000	0.0475	39.0392
537	302.9000	0.0475	46.8472
538	302.9000	0.0475	54.6552
539	302.9000	0.0475	62.4632
540	302.9000	0.0475	70.2712

Figure 10 Lumped Capacitance Matrix

3.4.3 Radiator Analysis

The radiator to which the heat sink is attached governs how effective the heat sink can get rid of heat. Several factors play a role in this. Equation 5 indicates that radiative heat flow is dependent on the surface emissivity, the radiator area, and the temperature difference between the radiator and the surroundings.

$$q_{rad} = \epsilon \sigma A_{rad} (T^4 - {T_{sur}}^4) \quad \text{Eq 9}$$

A variety of surface finishes exist for spacecraft applications with an array of values for emissivity [22]. Selecting a finish with a high emissivity will maximize radiative heat transfer into space for the given conditions, as will increasing the radiator surface area.

From a heat transfer perspective, the heat sink is in contact with the radiator so that heat is conducted from the heat sink wall into the interior radiator wall, through the thickness of the radiator, and finally radiated into space. Based on conductive thermal resistance,

$$R_{cond} = \frac{L}{k} \quad \text{Eq 26}$$

where *L* is the distance in the direction of heat flow and *k* is thermal conductivity, minimizing *L* and maximizing *k* will reduce the resistance through the radiator. Minimizing the thermal resistance will maximize the radiator surface temperature and maximize heat transfer into space.

3.4.4 System Tools Kit

STK provided information about contact times between a cubesat and the several ground stations that comprise the MC3 network. Establishing sensors in the various locations and setting an orbit for a satellite, STK provided the ground contact data over the course of 31 days. This ground contact data consists of the start and stop time for each ground contact during the entirety of the simulation. This data could be read by a modified version of the lumped capacitance model to provide a theoretical temperature

profile of a gallium heat sink over this time span. This model assumes that the radio is transmitting for the full duration of each ground contact.

3.5 Laboratory Testing

This study made use of a thermal vacuum chamber to study the radiative characteristics of the PCM heat sink. The atmosphere inside a chamber can be removed to create an adequate vacuum while the chamber's interior walls can be temperature controlled for heat transfer applications a space vehicle may encounter. A heater, applied to one side of the sink, applied approximately 10 Watts of heat into the heat sink for a certain period of time. After this time, heat was allowed to radiate out of the heat sink into the walls of the thermal vacuum chamber. Thermocouples attached to the heater and the heat sink provided a means of collecting temperature data during the experiment in order to build temperature profiles that show the temperature dependent on time. The profiles indicate the time required for the heat sink to reach the melting point of gallium, how long the heat sink remained at a constant temperature due to the phase change, the peak temperature, and the time required to radiate the heat away.

In addition to the scenario above, scenarios involving an entire phase change of the gallium were conducted in similar fashion. An entire phase change can be achieved either by increasing the time the heater operates, increasing the output of the heater, or a combination of both. The benefit of a total phase change, or a total change from solid to liquid, is that the effects of supercooling, if any, can be studied since supercooling is more likely to occur when no solid gallium remains present in the heat sink. In addition to the information provided in the temperature profiles mentioned previously, the

temperature profiles also indicate if supercooling occurs as the heat sink temperature will not remain constant as the gallium reaches its melting point during the cooling period. Furthermore, the temperature profile will also show when solidification of supercooled gallium occurs since the temperature will quickly increase to the melting point and remain constant for a period of time until solidification is complete.

3.5.1 Test article

A complete test article consisted of several parts: a heat sink, a flat radiator plate, an insulator, four thermocouples, and a film heater. The thermocouples and heater were each placed in identical locations across each test article. Five different heat sink/radiator combinations were available for testing.

3.5.1.1 Heat sink filling procedure

A process was developed to fill the heat sinks with gallium. Prior to filling, a 1/16 inch pipe plug wrapped in thread seal tape was installed in the lower port of each heat sink. Two beakers were filled halfway with water and, using a hot plate, heated to approximately 120 degrees Fahrenheit. An empty heat sink was placed in one beaker and two vials of gallium were placed in the other beaker. Once the gallium was entirely melted, it was then poured into the heat sink via a small funnel and a 1/8 inch pipe plug wrapped in thread seal tape was installed into the top filling port. This process was performed for all six heat sinks.

3.5.1.2 Radiator

Six radiator plates were fabricated out of aluminum at the AFIT machine shop. Aluminum was chosen due to its high thermal conductivity and low thermal resistance so

that heat would pass easily from the heat sink into the radiator plate. All plates were identical in dimension (100mm x 100mm x 3.2mm). Three radiators plates were left uncoated in bare aluminum while the other three radiator plates were sent to Alpine Metal Finishing to be coated in Aeroglaze® Z276 white paint. This was done to maximize the radiator's emissivity for vacuum chamber testing. Each radiator was fabricated with mounting holes that lined up with those of the heat sink to assist in ensuring proper alignment during the heat sink mounting process as well as to provide consistent placement among the test articles.

3.5.1.3 Insulator

In order to encourage heat to flow in one direction through the test article, an insulator was developed. To ensure compatibility and proper fit with the heat sink and radiator, a prototype was additively manufactured at AFIT using polylactic acid (PLA). After a fit check, slight dimensional modifications were made to the insulator. For laboratory testing purposes, three identical insulators were manufactured by Stratasys out of ULTEM 9085 via the FDM process (see Figure 11).

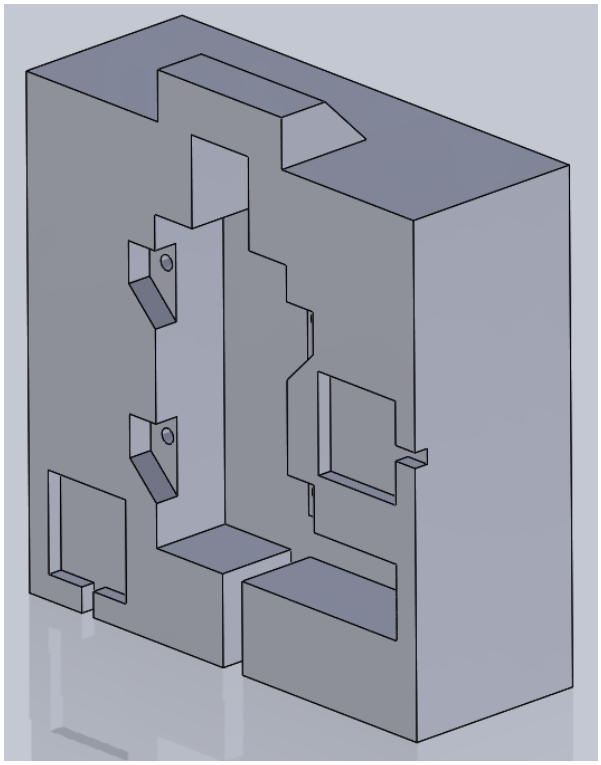

Figure 11 Insulator as designed by the author

Assuming heater output was 10 Watts, the heat loss through the insulator was estimated to be between 0.33 and 1.65 Watts depending on the temperature. A small gap exists between the heat sink and the insulator, thus radiation is the prime mechanism of heat transfer between the two entities. However, for simplicity, the difference in temperature between the heat sink and the insulator was assumed to be negligible. Table 3 shows the estimated exterior temperature of the insulator based on the heat sink temperature as well as the estimated heat loss in Watts.

Table 3 Estimated Heat Losses

Heat Sink Temp (K)	Insulator Exterior Temp (K)	Watts
310	291	1.65
303	286	1.39
290	279	0.91
280	273	0.56
273	269	0.33

3.5.1.4 Thermocouples

K-type thermocouples, product # TC40KT40A, were purchased from MINCO Products, Inc. The test article was designed to accommodate up to four thermocouples at once. Two thermocouples could be placed on the back of the radiator; one near the lower left corner and one on the middle right side. A third thermocouple was placed on the heat sink adjacent to the heater and the fourth was located on the front of the radiator in the center.

3.5.1.5 Heaters

In addition to the thermocouples, polyimide film heaters were purchased from MINCO Products, Inc. The heaters, part # HK6907, measured 1 x 2 inches and featured adhesive for easy installation. The advertised resistance was 47.78 Ohms with a ±10% tolerance band (43 Ohms to 52.55 Ohms) and an advertised temperature range of 240K to 373K [23]. The temperature coefficient of resistance, or TCR, for this type of heater is very low, with typical values of about 0.0005 Ω/Ω/ºC [24]. Due to such a low TCR, the electrical resistance-to-temperature profile for these heaters can be assumed flat with negligible change in electrical resistance over the temperature range [25]. However, even though these heaters were advertised with a low TCR value, a change in temperature will

result in a subtle change in resistance. The following equation relates changes in temperature to changes in electrical resistance [26]:

$$R = R_{ref}[1 + \alpha(T - T_{ref})] \quad \text{Eq 27}$$

where *R* is *Resistance (Ohms)*, R_{ref} is *Reference Resistance (Ohms)*, α is *TCR*, *T* is *conductor temperature (Kelvin)*, and T_{ref} is *Reference Temperature (Kelvin)*. It should be noted that *T* and T_{ref} can be in either degrees Celsius or Kelvin, as long as they are consistent with each other. Table 4 shows the resistance values calculated using Eq 27 above as well as the percent error from the advertised resistance over the temperature range that was experienced during the experiments. The reference temperature used in the calculation was 20 ºCelsius (293 Kelvin) while the reference resistance was the advertised 47.78 Ohms.

Table 4 Temperature vs Resistance

Temperature (Kelvin)	Resistance (Ohms)	% Error in Resistance
263	47.06	1.50%
273	47.30	1.00%
283	47.54	0.50%
293	47.78	0.00%
303	48.02	0.50%
313	48.26	1.00%

The resistances of five heaters were measured at room temperature and the average resistance was 47.13 Ohms. The average resistance of the entire circuit (the heater and the two wires connecting it to the power supply) was 47.32 Ohms (see Table 5).

Table 5 Measured Resistances

Heater	Heater Resistance (Ohms)	Full Circuit Resistance (Ohms)
1	47.73	47.90
2	47.13	47.33
3	46.56	46.77
4	47.67	47.85
5	46.54	46.73
Average	47.13	47.32

One heater was applied to the back of each heat sink. In order to produce the desired 10 Watt output, the voltage of the power supply to which the heater was connected was determined using the following equation:

$$V = \sqrt{P * R} \qquad \text{Eq 28}$$

where V is voltage, P is power in Watts, and R is the resistance in Ohms. The resistance of each heater was measured prior to testing to determine the proper voltage to produce approximately 10 Watts. It should be noted that only the resistance of the heater was used to determine the voltage for the trials. The resistance of the two wires between the heater and the power supply was omitted in the calculation. However, its inclusion in the calculation would have had a minimal impact. From Table 5, it is clear that the two wires have an average resistance value of about 0.19 Ohms, which equates to approximately 0.04 Watts being dissipated through the wires. Thus, neglecting the wires contributed approximately 0.4 percent error to the experiment.

3.5.2 Atmospheric Testing

3.5.2.1 Full-Melt Test

The purpose of the atmospheric full-melt test is to experimentally determine the characteristics of the melting and freezing processes with a test article at ambient temperature and pressure. The test begins with the test article at ambient temperature. The film heater applies a heat flux into the heat sink until the melting process has concluded and the maximum temperature has been obtained. At this point, the heater is turned off and the assembly is allowed to cool. Once solidification concludes, the assembly will continue to cool until it has reached ambient temperature.

3.5.3 Vacuum Testing

3.5.3.1 Full-Melt Test

The purpose of the vacuum full-melt test is to experimentally determine the characteristics of the melting and freezing processes with a test article subjected to a vacuum environment with the temperature of the surroundings at 263 Kelvin in order to simulate a space environment. Similar to the atmospheric full-melt test, the vacuum full-melt test begins with the test article near ambient. The heater applies a heat flux into the heat sink until the melting process has concluded and the maximum temperature has been obtained. Power is removed from the heater and the heat sink is allowed to cool until it reaches ambient.

3.5.3.2 Fifteen Minute Melt Test

Similar to the Full-Melt Test, the purpose of this partial melt test is to experimentally determine the phase change characteristics with a test article subjected to

a vacuum environment with the surrounding temperature at 263 Kelvin. With the test article near ambient temperature, the heater applies a heat flux to the heat sink for 15 minutes. Once this time has passed, power is removed from the heater and the test article is allowed to cool. This test seeks to simulate a partial melt, which is what a heat sink on board a satellite would most likely encounter.

3.6 Month-Long Orbit Simulation

Using the Lumped Capacitance Model, the orbit simulation places the heat sink in a scenario it might encounter in low earth orbit. Assuming the interior of the satellite is a constant 24° Celsius, the simulation produces the temperature profile of the heat sink based on the contact times produced in STK. This simulation is intended as a tool to be used in the design of a gallium PCM heat sink in order to optimize the volume of gallium to be used in a mission.

3.7 Summary

This chapter put forth the methodology used in this research. A PCM heat sink was designed based on the footprint of an AstroDev Lithium 1 radio and several were manufactured: two from 316 stainless steel, two from Inconel 718, and two from ULTEM 9085. These heat sinks were used as the test articles for this research and thermal profiles were created based on the temperature data obtained from laboratory testing. Heat transfer models were created in MATLAB for each material in order to characterize the behavior of the system.

Since the product of this thesis is to develop a process for designing and manufacturing an additively manufactured PCM heat sink, the different materials needed

to be compared to each other. Each heat sink material has a different thermal conductivity. As such, each heat sink will have a unique temperature profile. As part of the analysis process, the effectiveness of the heat sinks were analyzed alongside the cost and difficulty of the manufacturing for each. Chapter 4 presents the results of this testing.

IV. Analysis and Results

4.1 Chapter Overview

This chapter presents the results of the simulations along with the data collected from laboratory testing. The information presented here seeks to demonstrate the feasibility of gallium as a PCM for the passive thermal management for space vehicles.

4.2 Test article Masses

Table 6 shows the masses of each empty heat sink, the mass of the gallium within it, and the mass of the radiator to which each heat sink was attached. The average mass of gallium per heat sink was 93 grams. During the filling processes, it was discovered that residual gallium remained in the vials and was difficult to remove.

Table 6 Test article masses

Heat sink identification and material	Heat sink empty (grams)	Heat sink full (grams)	Ga Mass (grams)	Radiator Mass (grams)	Total Mass (grams)
IN 1 (Inconel 718)	91.1*	183.6	92.5*	81.4	265
IN 2 (Inconel 718)	91.1	185.3	94.2	84.3#	269.6
SS 1 (Stainless Steel 316)	87.0	179.9	92.9	81.4	261.3
SS 2 (Stainless Steel 316)	87.1	181.4	94.3	84.2#	265.6
UL 1 (ULTEM 9085)	24.0	116.1	92.1	84.2#	200.3
UL 2 (ULTEM 9085)	24.0	116.1	92.1	Not tested	

* IN 1 was not weighed empty. The estimated mass of gallium in this heat sink was determined using the empty mass of IN2.

Includes mass of Aeroglaze paint

Table 7 shows the equivalent masses and volumes of the non-metallic PCMs (shown previously in Table 1) that would be required to have the same available latent heat as 100 grams of gallium. While the required mass for each is significantly less than 100 grams, the volume of each is much larger than the 16.9 milliliters that the gallium occupies. The volume ratio shows how many times larger the volumes for these PCMs would be in place of gallium. The last column shows the required heat sink depth needed to accommodate the PCM, assuming all other dimensions of the heat sink remain constant. The dimensions of the gallium heat sink are 32mm x 62mm x 12.7mm (*w x h x l)*. As shown previously in chapter 2, the thermal diffusivity is significantly less for each of these PCMs when compared to gallium.

Table 7 Equivalent non-metallic PCM volumes

PCM	Mass (g)	Volume (mL)	Volume ratio	Heat sink depth (mm)
S32	40.1	27.5	1.6	15.3
S30	42.2	32.4	1.9	18
S27	43.8	28.6	1.7	15.9
A32	61.7	73	4.3	40.6
A29	35.5	43.8	2.6	24.3
A28	51.7	65.5	3.9	36.4
A26	53.4	67.6	4	37.6

4.3 Laboratory Data

4.3.1 Atmospheric

The atmospheric trials sought to demonstrate the ability to conduct the testing and to ensure all equipment was functioning properly. For these trials, each test article was

tested one at a time in the vacuum chamber at ambient temperature and pressure. All of the four thermocouples on each test article were utilized in every trial. For the atmospheric testing, five full-melt test profiles were performed using the stainless steel, Inconel, and ULTEM heat sinks. Figure 12 through Figure 14 show the data collected from the thermocouple attached to the rear of the heat sink adjacent to the heater.

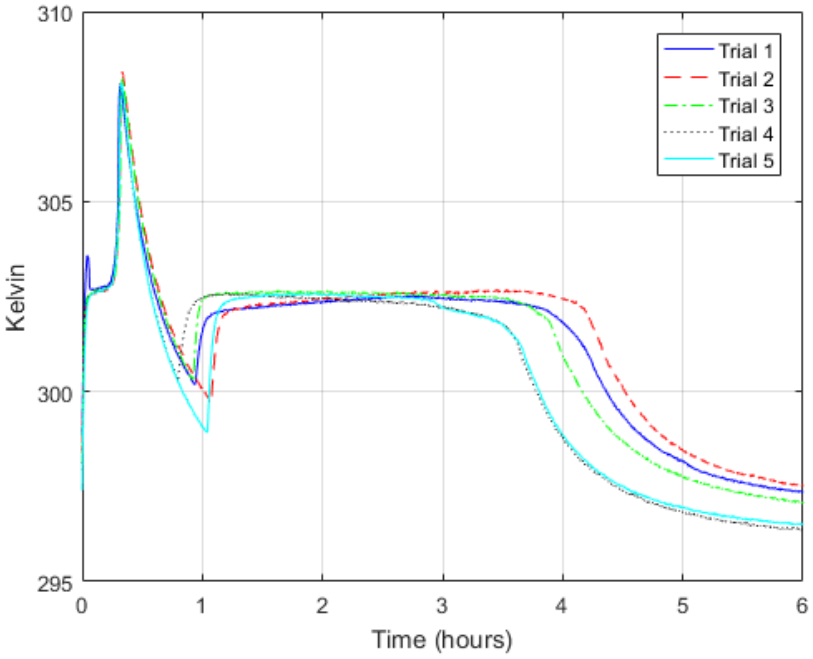

Figure 12 Stainless Steel Atmospheric Full Melt Trials

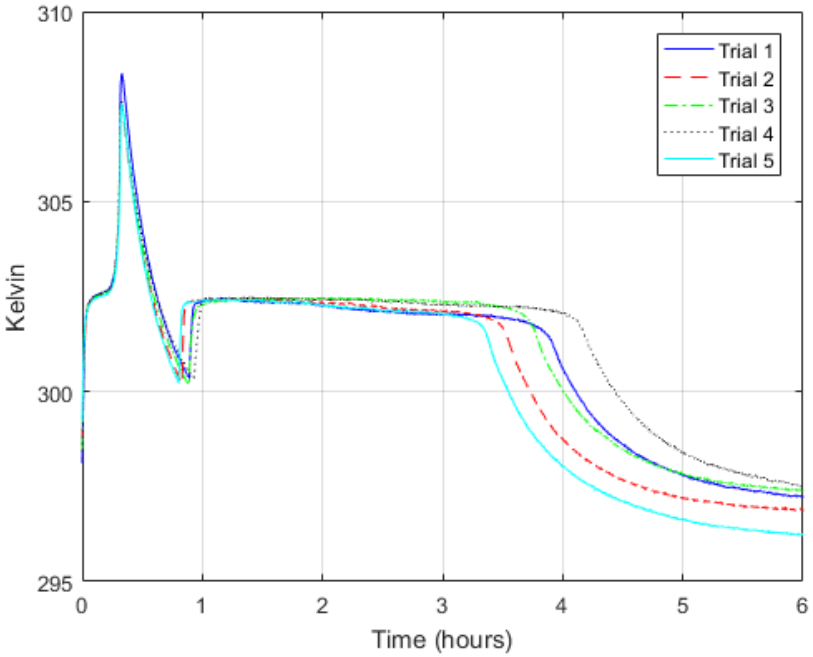

Figure 13 Inconel Atmospheric Full Melt Trials

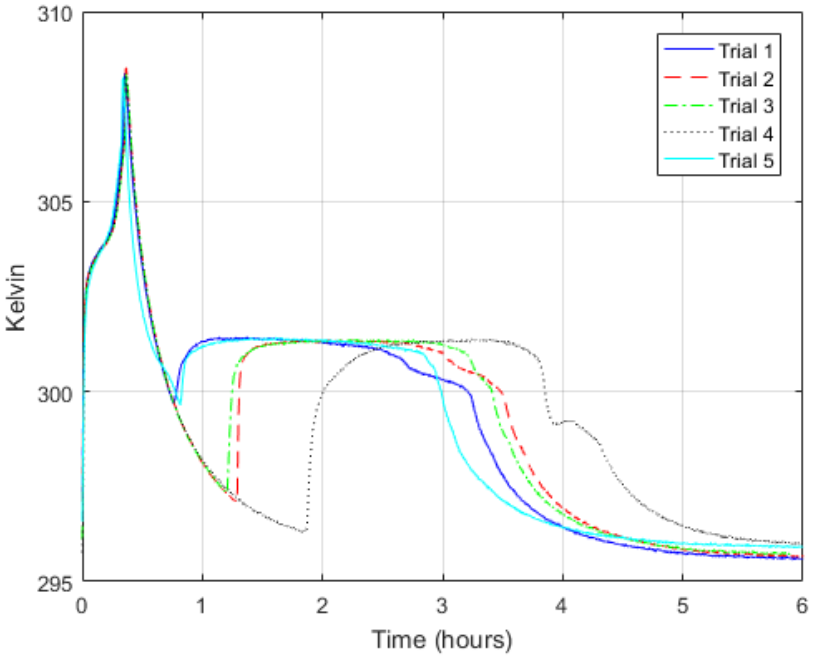

Figure 14 ULTEM Atmospheric Full Melt Trials

Each of the three previous figures effectively shows the sensible heating from the initial temperature up to the melting point, where the temperature levels off and remains fairly constant for the duration of the phase change. This is demonstrated in the stainless steel and Inconel heat sinks more so than in the ULTEM heat sink, probably due to ULTEM's much lower thermal conductivity compared to that of the two metals. Also shown is the continued increase in temperature at the end of the phase change. Once the power supply was switched off, the temperature continued to climb for several seconds until leveling off and, finally, decreasing. This increase was mostly likely due to the heater temperature remaining higher than the heat sink wall for the several seconds after switching off. Supercooling is seen in every trial for the three heat sinks as the temperature decreases from its peak and drops below the melting point without undergoing a phase change. Supercooling causes solidification to begin somewhat spontaneously and is demonstrated where the temperature quickly increases to the melting point and remains constant during the solidification process. Once solidification is complete, the temperature again begins to decrease until it approaches ambient.

4.3.2 Vacuum Testing

4.3.2.1 Full-Melt Trials

Testing in an evacuated environment was performed in order to more closely simulate what the heat sink might see in space. The full melt profiles were conducted first and in similar fashion as the atmospheric full melt profiles, with the exception that two test articles were tested simultaneously and only three thermocouples were used per test article. The data collected from the stainless steel heat sink trials is presented in

Figure 15. This figure portrays the data collected by the thermocouple attached to the rear of the heat sink adjacent to the heater. Figure 16 shows the heat equation model and the lumped capacitance model at that thermocouple location as well as laboratory data for comparison. The vertical red line indicates power shutoff.

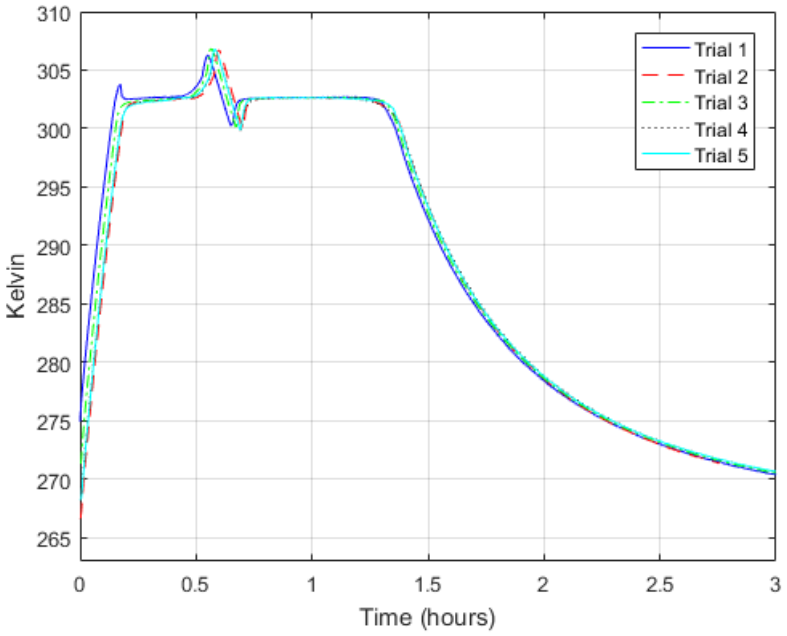

Figure 15 Stainless Steel Vacuum Full Melt Trials

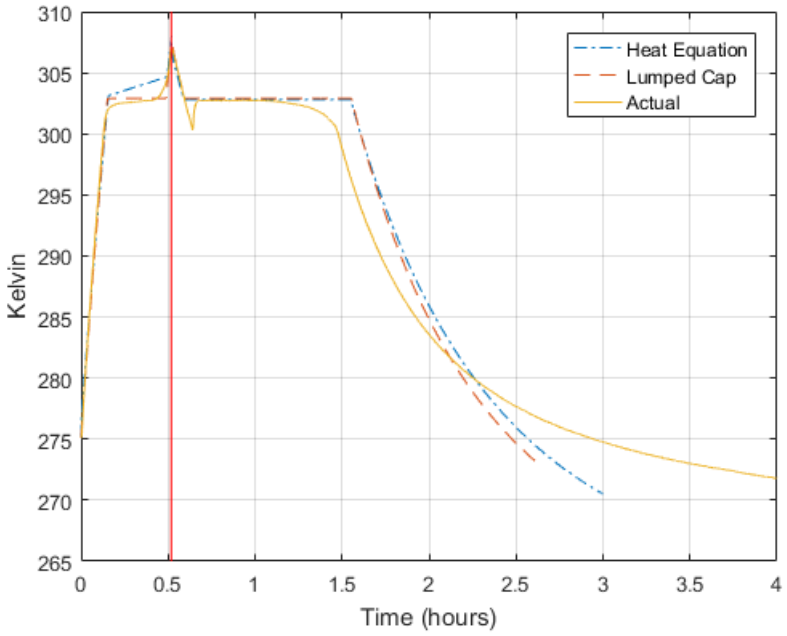

Figure 16 Stainless steel full melt models

The preceding figures show that the heat equation model and the lumped capacitance model agree with each other to a high degree. Further, both models show that they can emulate the laboratory data reasonably well. However, supercooling presents divergence between the model and the measured data. The model does not account for supercooling, but instead proceeds into the solidification phase as it approaches the melting point during cooling. Once the solidification phase is complete, the cooling portions of the model and lab data display similar trends. Furthermore, the laboratory data shows that the gallium solidified more quickly than what either model predicted. The models assume heat is allowed to escape only through the radiator plate. Referencing back to section 3.5.1.3, the estimated heat loss through the insulator was between 0.33 and 1.65 Watts depending on the temperature. While the majority of the

heat was lost through the radiator, a small amount was lost through the insulator. This offers an explanation for why the test article solidified more quickly than the models.

The data collected from the Inconel heat sink trials is shown in Figure 17. Figure 18 shows the heat equation model and the lumped capacitance model as well as laboratory data for comparison. The vertical red line indicates power shutoff.

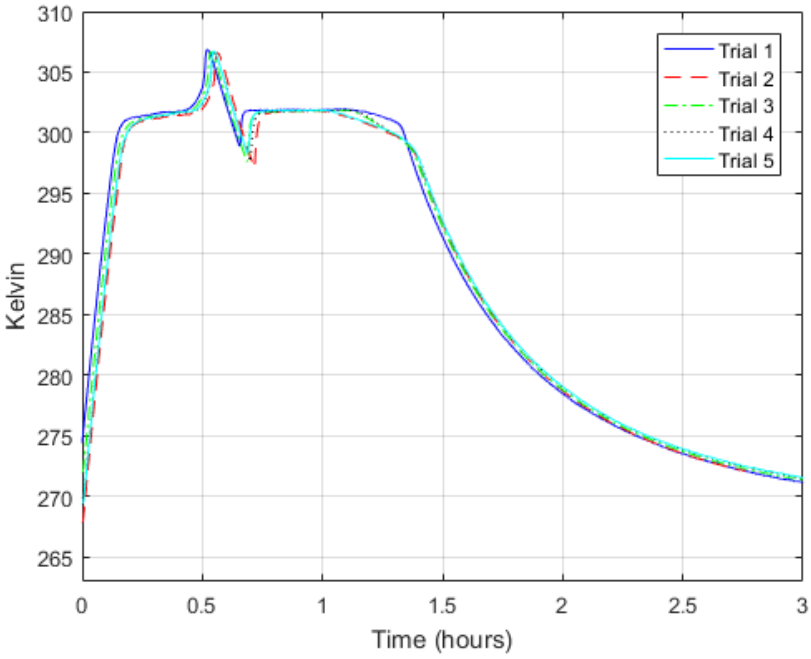

Figure 17 Inconel Vacuum Full Melt Trials

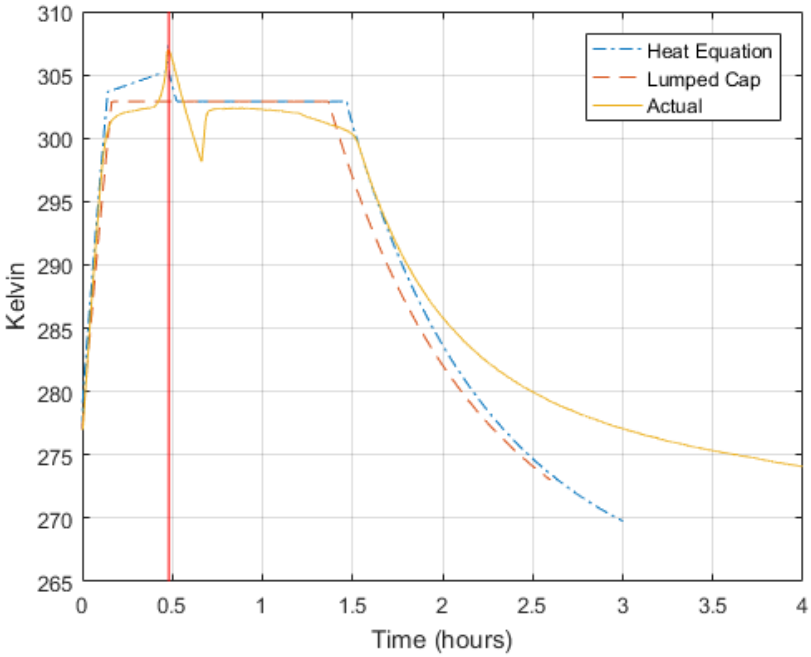

Figure 18 Inconel full melt models

The Inconel heat sink displayed similar characteristics as the stainless steel heat sink during the full melt trials. Like the stainless steel heat sink, there was similar agreement between the measured data and the two models.

4.3.2.2 Fifteen Minute Melt Trials

In addition to the full melt test profiles, partial melt test profiles were conducted in a similar fashion. The heaters were turned on for fifteen minutes, then powered down to allow the test articles to cool. As with the full-melt trials, two test articles were tested simultaneously and only three thermocouples were used per test article. The data collected from the stainless steel heat sink trials is shown in Figure 19. The models compared with measured data is shown in Figure 20.

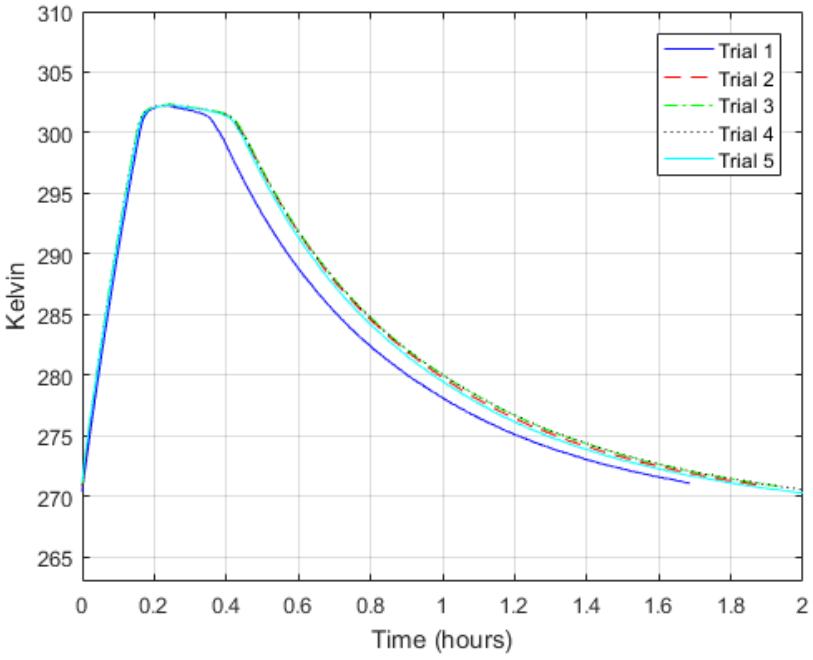

Figure 19 Stainless Vacuum 15 Minute Melt Trials

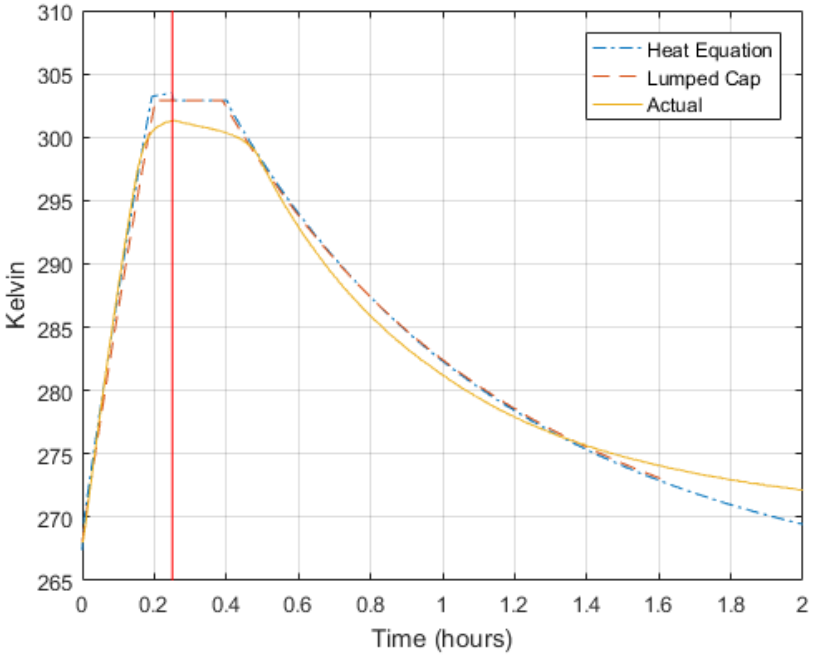

Figure 20 Stainless steel 15 minute melt models

The preceding figure depicting the 15 minute melt for the stainless steel heat sink shows that the heating and cooling portions of both models closely matches the laboratory data. Unlike the full-melt trials, supercooling is clearly absent in these partial melt trials. Since a portion of gallium remained solid during the phase change, supercooling was not expected to occur.

The data collected from the Inconel heat sink trials is shown in Figure 21. The models compared with measured data is shown in Figure 22.

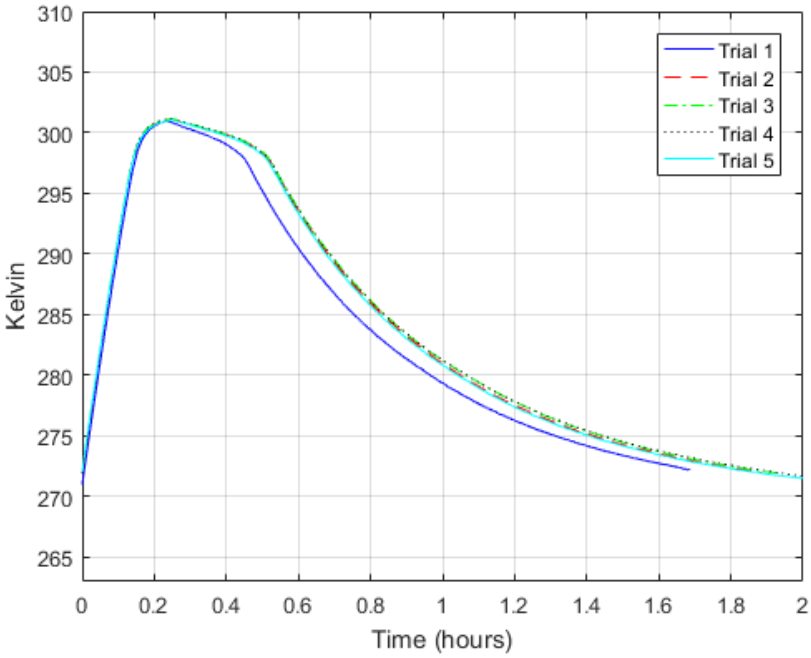

Figure 21 Inconel Vacuum 15 Minute Melt Trials

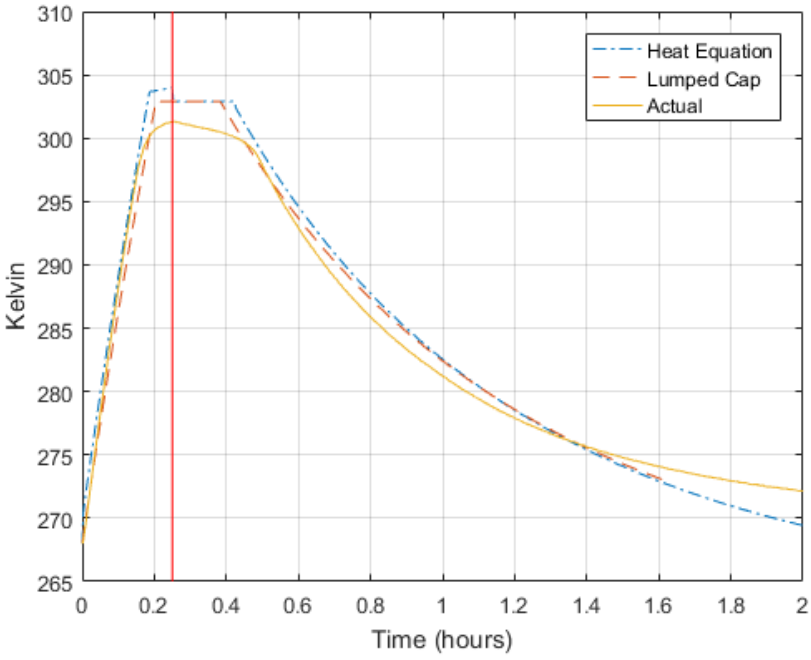

Figure 22 Inconel 15 minute melt models

The preceding figures depicting the 15 minute melt trials for the Inconel heat sink show again that the heating and cooling portions of the model closely matches the laboratory data. Also, supercooling is again absent in these partial melt trials and was not expected to occur.

4.3.3 Supercooling

As can be seen in the previous full melt trials, supercooling occurred in every test profile, illustrating gallium's strong tendency to supercool. While some variation does exist between trials, especially the atmospheric trials that were conducted at ambient, the metal heat sinks displayed a fairly consistent supercooling tendency. The ULTEM heat sink, on the other hand, had a much more variable nature in its supercooling tendency. The surface roughness (Figure 23) of the ULTEM heat sink was much different

compared to that of the Stainless Steel or Inconel heat sink (Figure 24 and Figure 25, respectively). The unique surface roughness of the ULTEM heat sink may have contributed to the spontaneity of the supercooling. The Stainless Steel and Inconel surfaces offer a large number of peaks compared to the ULTEM surface. These many peaks provide sites that can encourage nucleation of the gallium, which is consistent with the more predictable supercooling tendency with the metal heatsinks.

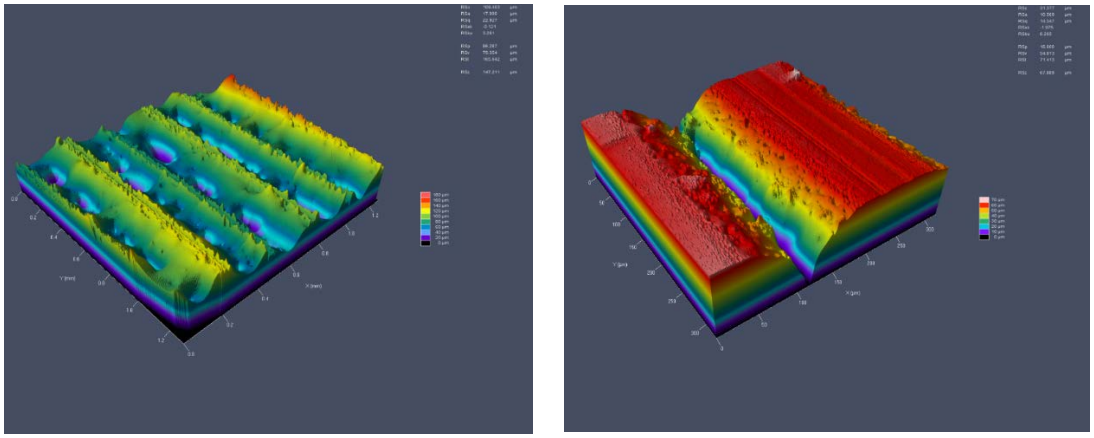

Figure 23 ULTEM 9085 5x (left) and 20x (right) Magnification

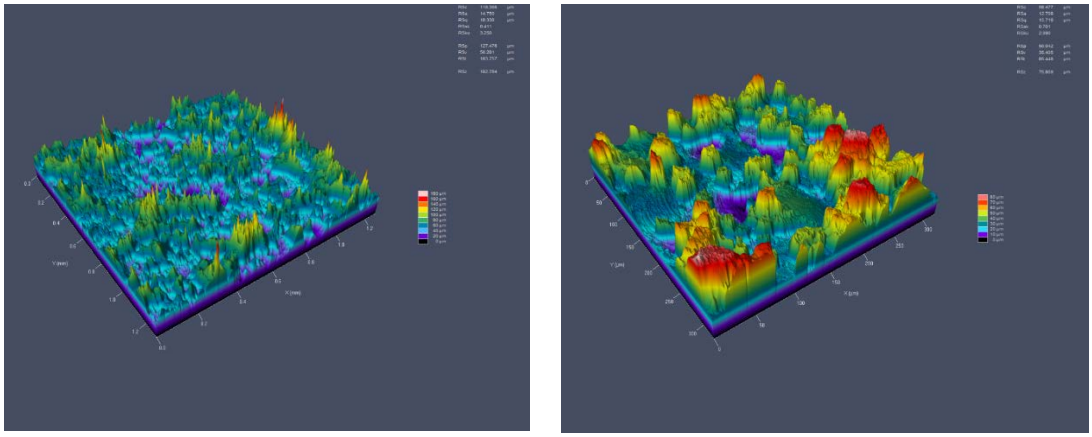

Figure 24 Stainless Steel 316 5x (left) and 20x (right) Magnification

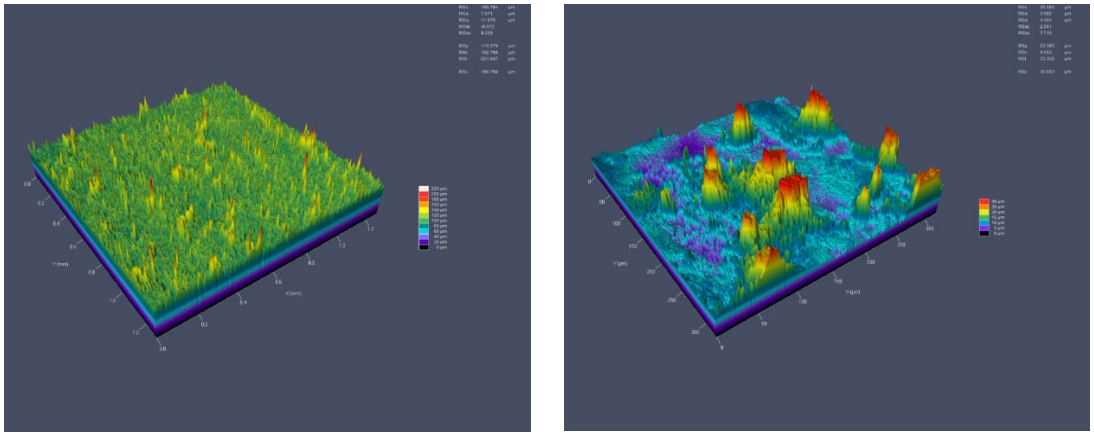

Figure 25 Inconel 718 5x (left) and 20x (right) Magnification

Referencing back to Figure 14 shows how supercooling can increase the amount of time required for the gallium to release its heat. The laboratory data for the ULTEM atmospheric trials shows that the solidification process took a little over two hours to complete for each trial. Even though each trial began with similar conditions, the supercooling that was experienced in each trial prolonged initiation of the solidification process. As a result, the amount of time required to cool back to ambient was also prolonged, with Trial 4 having the longest delay. Since the rate at which heat is transferred from the assembly to the surroundings is dependent on the temperature difference between the two, supercooling will naturally decrease the heat transfer rate, resulting in prolonged cooling times.

4.3.4 Gallium Leakage

Three of the heat sinks experienced leakage during the course of this research: UL 1, UL 2, and SS 2. After atmospheric testing, it was discovered that UL 1 had leaked in multiple areas, although it had displayed no containment issues prior to testing. UL 1 was not used in any subsequent testing. After UL 2 had been filled, it was discovered

that gallium was seeping through the base of this heat sink. Because leaking was noticed prior to testing, this heat sink was not used. Finally, SS 2 had leaked a small amount after vacuum testing had concluded. UL 1 and SS 2 both experienced leaks around the threaded areas and both ULTEM heat sinks experience leaks through the material itself. Given ULTEM 9085's lower tensile strength compared to either stainless steel or Inconel, the expansion that occurs during gallium's solidification would have a greater impact on the structural integrity of the ULTEM container as opposed to the metal containers.

4.3.5 Comparison to non-metallic PCMs

To illustrate the benefits of gallium as a PCM, the heat equation model was used to simulate the characteristics of two non-metallic PCMs in order to directly compare the types. Figure 26 shows the modelled temperature profiles of A29, S30 and gallium. For this comparison, the volume of each PCM was adjusted so that the total latent heat of fusion is equal between the three, approximately 8012 Joules. It should be noted that the model does not account for the use of TCEs for any of the materials. While gallium does not require them, the non-metallic PCMs would greatly benefit from their use. However, the lack of TCEs in the model was done in order to offer a more direct comparison between the gallium and the non-metallic PCMs.

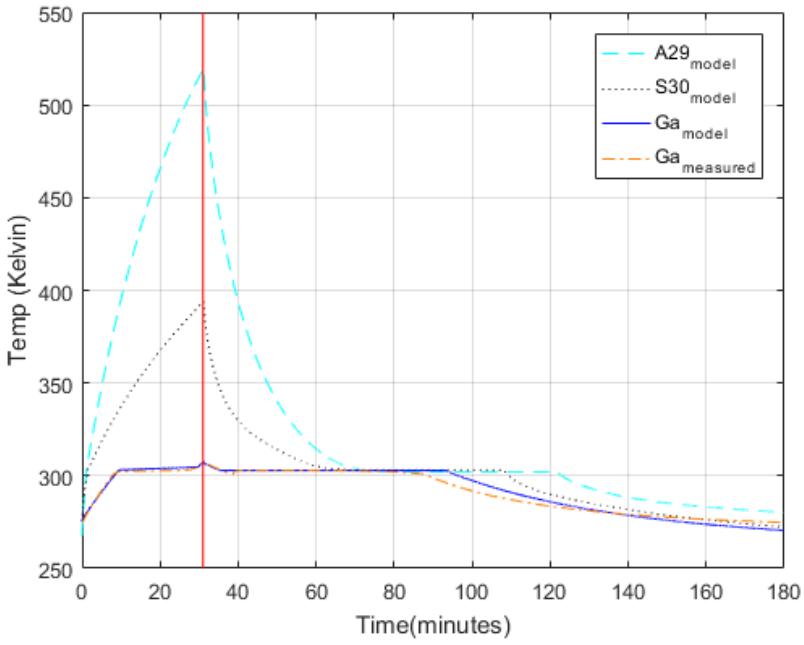

Figure 26 PCM Comparison

The temperatures shown are the temperatures at the heat sink wall. The advantage of gallium is apparent in this simulation. During the thirty-one minutes of heat input, the gallium maintained the lowest temperature by a significant margin. The S30 PCM attained approximately 390 K while the A29 reached more than 500 K. The ability to maintain this lower temperature helps to ensure the longevity of space vehicle electronics.

Also apparent from Figure 26 is the fact that A29 and S30 do not plateau at their melting points as gallium does. The slope of the temperature profile for these two PCMs starts out very steep until the melting temperature is reached. At that point, the slopes of the temperature profiles decrease as the PCMs undergo melting, but never take on a flat appearance as gallium does during phase change. This is due to the thermal

conductivities of A29 and S30 being significantly lower than gallium, which prevents the plateauing from occurring.

This phenomenon can be confirmed using the equation for conduction, Eq 1, mentioned previously in Chapter 2. Referencing back to this equation, it is easy to see that the temperature difference across some distance must increase as the thermal conductivity decreases, assuming all other variables are held constant. Given gallium's much higher thermal conductivity, its thermal resistance is low and allows heat to easily pass through the assembly. A29 and S30, having significantly lower thermal conductivities in comparison, have significantly higher thermal resistances as a result. This causes thermal energy to accumulate near the heat source and drastically increases the temperature at that location instead of passing easily through the assembly. It's worth noting that gallium's thermal conductivity is approximately 163 times and 61 times higher than that of A29 and S30, respectively.

Figure 27 through Figure 29 further illustrate the advantage of gallium over S30 and A29 in terms of maintaining a lower temperature. These figures show the simulated temperature distributions along the assembly at five minute time intervals over a thirty-five minute time span, with heat being applied for the first thirty-one minutes.

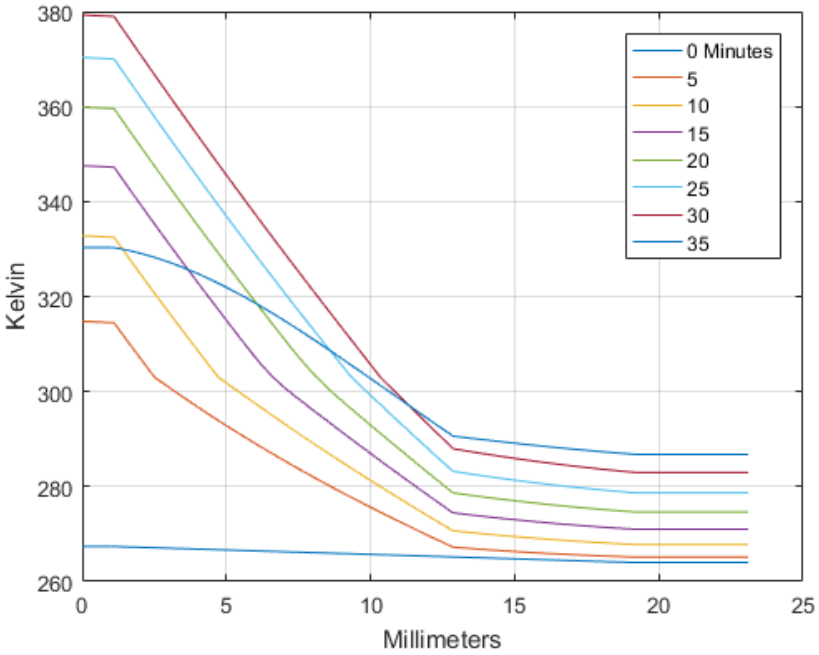

Figure 27 S30 Temperature Distribution at 5-Minute Time Increments

In Figure 27, a change in slope is apparent in each temperature distribution (except at 35 minutes) at approximately 303 Kelvin, which is the melting temperature of S30. This change in slope represents the boundary between the liquid and solid phases of the PCM and becomes less pronounced the longer heat is applied. The temperature distribution at thirty-five minutes takes on different shape compared to the distributions at previous time steps. The assembly has cooled for approximately four minutes resulting in a curved line as heat is removed.

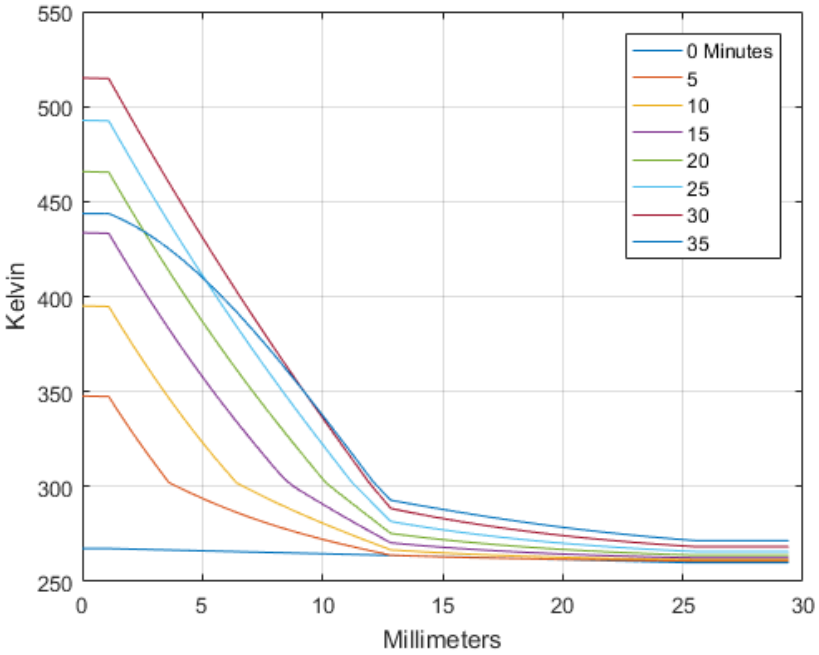

Figure 28 A29 Temperature Distribution at 5-Minute Time Increments

Figure 28 shows a pattern that is similar to that shown in Figure 27. Again, a change in slope is observed at the melting point of the material indicating the liquid-solid boundary, with the change being greater at lower time steps and becoming less obvious as time increases. The two previous materials show differences in their distributions at each time step due to the differences between their thermal properties.

Figure 29 shows much different temperature distributions than the previous two figures. The much higher thermal conductivity enables heat to easily flow through the assembly and produces temperature distributions with much smaller slopes. The liquid-solid boundary is also much less apparent as a result.

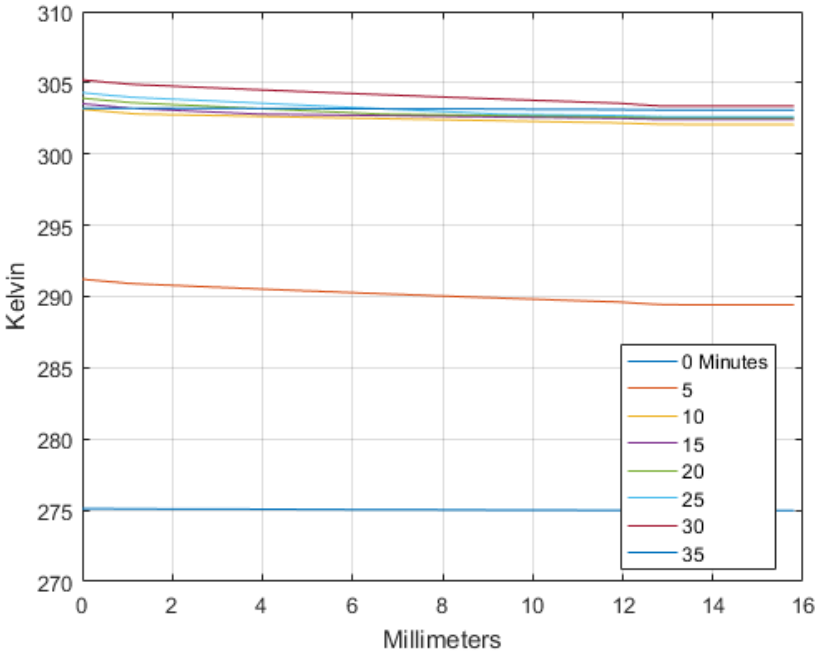

Figure 29 Gallium Temperature Distribution at 5-Minute Time Increments

4.4 Month-Long Orbit Simulation Results

The theoretical temperature profile for the stainless steel heat sink of the 31 day simulation is shown in Appendix B. For this simulation, a circular orbit at 600 km with an inclination of 60 degrees was programmed using STK, with the MC3 network being used for the ground station locations. Over the course of the 31 days, the satellite had 151 contacts with the various ground stations with contact times ranging from 24 to 160 seconds. At certain points, the time between contacts was very short, on the order of a few seconds. At other points, the contacts between stations overlapped, effectively

creating one long contact time from the point of view of the satellite's radio in either of these cases.

The graphs show how the phase change process prevents excessive temperatures. In many instances, the radio does not transmit long enough for excessive temperatures to be a problem. These instances are illustrated when the temperature does not reach the melting point. In other instances, the radio transmits long enough to transfer ample heat into the gallium to begin melt it. However, based on the current parameters used for this simulation, the temperature never exceeds gallium's melting point. This illustrates that the gallium never completely melts during the simulation. This simulation seeks to demonstrate the usefulness of being able to predict the temperatures the heat sink will encounter. Using this model in the design of the heat sink offers a method of determining the optimal mass of gallium for a particular design.

4.5 Investigative Questions Answered

Both of the heat transfer models developed for this research demonstrated their usefulness in predicted the behavior of the phase change and the sensible heating. In terms of designing a gallium PCM heat sink, the models appears to offer a reasonable estimation of the temperature profile that the heat sink will experience in orbit. While the heat equation model can offer much more information than the lumped capacitance model can, the lumped capacitance model was shown to highly agree with the heat equation model was predicting.

4.6 Summary

This chapter presented the results of laboratory data and simulations and compared the two to verify the accuracy of the model, as well as the potential of using it as a tool in the design of a heat sink to fit a particular application. The laboratory testing provided detailed information on the phase change that occurs within the heat sink. The supercooling phenomenon was demonstrated and revealed a high probability of occurrence when the gallium was fully melted. Also, the supercooling demonstrated the spontaneity of freezing initiation and how the heat sink material may have an impact on it. The data presented in this chapter demonstrated that gallium as a PCM has potential in satellite thermal management.

V. Conclusions and Recommendations

5.1 Chapter Overview

This research has demonstrated that gallium as a phase change material can offer a simple solution to the challenges of thermal management in space vehicles. This chapter puts forth the conclusion of this research, its impact, and recommendations for future research.

5.2 Conclusions of Research

The lumped capacitance model that was developed for this research demonstrated that it could be used in designing a heat sink for a particular need. Even though the solidification process simulated in the model deviated from the laboratory testing, in every case the actual test article solidified more quickly than the simulation showed. Further refinement of the lumped capacitance model may increase accuracy and therefore reduce margin and optimize the volume of gallium.

For research purposes, a mass of 100 grams of gallium was chosen. However, in the design of a heat sink to be used in a space mission, the volume of gallium must be determined from the environment it will encounter. With mass and volume being critical design elements of satellite subsystems, selecting the proper mass is very important. The process for designing a gallium PCM heat sink is as follows:

- Determine the mission
- Design the orbit and space vehicle around the mission
- Determine contact time between satellite and ground stations

- Determine optimized volume of gallium based on contact times and contact frequency as well as output heat from the radio
- Design a heat sink based on radio footprint and the needed volume of gallium

5.3 Impact of Research

PCMs offer a method of thermal management where simplicity is of the utmost importance in the design. Much research has been conducted in the areas of non-metallic PCMs and while they have been utilized in previous applications, they have potentially inadequate qualities in comparison to gallium as a PCM for thermal management. This research presented the benefits of gallium in addition to laboratory data depicting actual temperature profiles of gallium's phase change. Additionally, this research presented a design of a heat sink based on an actual space vehicle communications radio as a proof of concept and demonstrated that this design could be additively manufactured with various materials and that the manufacturing was repeatable. Furthermore, the lumped capacitance model created for this research demonstrated its usefulness as a tool in designing a heat sink based on particular space mission requirements.

5.4 Recommendations for Future Research

While this research sought to determine the effectiveness and feasibility of gallium PCM heat sinks, areas for further research exist. While the aim is to use gallium PCM heat sinks for passive thermal management for satellite electronics, there exists several aspects that should be considered.

The material or materials used in the heat sink device play an important role into how well it will work. Having a high thermal conductivity, or at least high enough, so that heat can easily pass from the source, through the PCM, and out into space is one factor that determines the effectiveness. A second factor is the compatibility of the heat sink material with the gallium that it will contain. While Stainless Steel 316 and Inconel 718 appear to contain gallium well, their weight may be detrimental in space vehicle applications. While aluminum can be additively manufactured and has a desirable thermal conductivity, it will not be effective at containing gallium. In addition to metals, ULTEM has desirable properties for space vehicle applications. The gallium seepage encountered during laboratory testing cannot yet be solely attributed to the ULTEM itself. Since the ULTEM heat sinks were manufactured from the same design as that used for the metal heat sinks, the design may have played a role in why seepage occurred. The thickness may have been sufficient for the metal heat sinks while inadequate for the ULTEM in containing the gallium, potentially due to non-uniform stresses induced during solidification and separating the layers of ULTEM. Thus, a variety of materials should be researched for the following characteristics for use as gallium PCM heat sinks:

- compatibility with gallium (low reactivity)
- thermal conductivity and density
- ability to be additively manufactured
- porosity and minimum material thickness to prevent seepage

In parallel with researching heat sink materials, supercooling can potentially present undesired operation. As was demonstrated in laboratory testing (see Figure 14), the

ULTEM heat sink was much more spontaneous with supercooling than the either the stainless steel or the Inconel. The amount of extra gallium required to prevent supercooling for a particular scenario as well as the tradeoff of lighter-weight materials versus those materials' effects on supercooling spontaneity should be researched.

A third topic for future research is the phase change process. Chapter four compared simulations with actual laboratory data and showed how they matched as well as differed. The heating and melting portions were reasonably close between the two. However, the test articles always completed the solidification process before the model did. The amount of energy entering the gallium for it to completely melt should equal the amount of energy leaving the gallium in order for it to completely solidify, which was how the phase change was established in the model. The gallium in this research could not be directly observed as it was fully enclosed within the heat sink and any anomalies that may have occurred during the phase change process could only be inferred.

Lastly, a topic that should be considered for future research is the integration of gallium heat sinks into cubesat chassis with the various space vehicle electronics that will encounter transient operation while in orbit (e.g. transmitters). Furthermore, vibration testing of heat sinks should be conducted with the gallium in both solid and liquid phases as well as research of the fluid dynamics of liquid gallium subjected to such vibrations.

5.5 Summary

Thermal management is crucial to the longevity of space vehicle electronics, and as a result, the overall mission. The simpler the management system is, the higher the reliability of this system will be. The phase change system offers an avenue to a highly

reliable and very simple approach to controlling temperatures on a space vehicle. Furthermore, the unique properties of gallium as a phase change material offer particular advantages over non-metallic phase change materials. This research has demonstrated the function of such a device through modeling and laboratory testing. Finally, this research has presented the steps involved in designing and fabricating an additively manufactured gallium PCM heat sink for space vehicle applications.

Appendix A: MATLAB Code

Code for Heat Equation Model

```
%Heat Equation model
clear all, close all, clc

T0 = 277.01; %initial temp, K
T_sur = 263; %Kelvin, vacuum chamber wall temp
t = 180; %minutes, simulation time
tt = 1870;  %minutes * seconds, radio transmit time
q_rad = 8.4; %Watts, in
q_stby = 0; %Watts
dt = 0.0001; %sec
dx = 0.0001; %m

% heatsink
k_hs = 6.5; %W/m-K, thermal conductivity  SS=15, IN= 6.5
rho_hs = 8192; %kg/m^3, density    SS = 7970, In = 8192
c_p_hs = 435; %J/kg-K, specific heat    SS = 510, IN = 435
alpha_hs = k_hs/(rho_hs*c_p_hs); %thermal diffusivity of SS316
Fo_hs = alpha_hs*dt/dx^2; %Fourier number

%Solid PCM
l = .0107; %depth of PCM
L = l+.005; %meters, total depth of heat sink and radiator in x-
direction
%heatsink walls are 1mm each and radiator is 3mm.  5mm total
k_solid = 29.4; %W/m-K thermal conductivity
rho_solid = 5907; %kg/m^3 density
c_p_solid = 374; %J/kg-K  specific heat
alpha_solid = k_solid/(rho_solid*c_p_solid); %thermal diffusivity solid
gallium
Fo_solid = alpha_solid*dt/dx^2; %Fourier number

%Liquid PCM
T_melt = 302.9; %K, melting point of gallium
mass_Ga = 92.5; %grams    SS = 94.3, IN = 92.5
hof = 80.12; %Joules/gram, latent heat of fusion
Hmax = hof*mass_Ga/single((l/dx)); %total latent heat per node,  Joules
k_liquid = k_solid; %thermal conductivity
rho_liquid = 6095; %density
c_p_liquid = 373;  %specific heat
alpha_liquid = k_liquid/(rho_liquid*c_p_liquid); %thermal diffusivity
liquid gallium
Fo_liquid = alpha_liquid*dt/dx^2; %Fourier number

%Aluminum 7075
k_al = 130; %thermal conductivity
rho_al = 2800;  %density
c_p_al = 960;  %specific heat
```

```
alpha_al = k_al/(rho_al*c_p_al);  %thermal diffusivity
Fo_al = alpha_al*dt/dx^2; %Fourier number

in = single(L/dx+1); %# of nodes including zero
it = single(1/dt+1); %# of time steps (1 second per iteration)

epsilon = 0.95;  %emissivity of radiator
sigma = 5.670E-8; %W/m^2-K^4, Stephan-Boltzman constant
area_h = .032*.062; %area of heater
area_r = .0112; %radiator face and sides: 10x10 cm^2 face, 3mm thick
sides,

%%Initial Temp

%% Initial Temp Distribution

%Heat sink
L_ss = .001; %meters, length of hs wall
R_ss = L_ss/(k_hs*area_h); %thermal resistance through hs wall

%PCM
L_ga = l; %meters, length of PCM
R_ga = L_ga/(k_solid*area_h); %thermal resistance through PCM

%Aluminum 7075
L_al = .003; %meters, radiator thickness
R_al = L_al/(k_al*area_r); %thermal resistance through radiator

%To determine exterior radiator wall temp, an iterative process is
performed.
T5_x = T_sur; %Radiator Temp is initially set to be equal to the
surrounding temp.
q_out = epsilon*sigma*area_r*(T5_x^4 - T_sur^4);  %supposed heat flow
out based on temp
R_rad = 1/((epsilon*sigma*(T5_x+T_sur)*(T5_x^2+T_sur^2))*area_r);
%thermal resistance based on temp
R_tot = R_ss + R_ga + R_ss + R_al + R_rad; %total thermal resistance of
circuit
q = (T0 - T_sur)/(R_tot); %supposed heat flow through circuit
x = q - q_out; %difference between

while x > 0
q_out = epsilon*sigma*area_r*(T5_x^4 - T_sur^4); %heat flow out based
on radiator temp
T2 = T0 - q_out*R_ss; %temp at 1st interior wall
T3 = T2 - q_out*R_ga; %temp at 2nd interior wall
T4 = T3 - q_out*R_ss; %temp at interior radiator wall
T5 = T4 - q_out*R_al; %temp at exterior radiator wall
R_rad = 1/((epsilon*sigma*(T5+T_sur)*(T5^2+T_sur^2))*area_r); %thermal
resistance of radiator
R_tot = R_ss + R_ga + R_ss + R_al + R_rad; %thermal resistance of
circuit
```

```
q = (T0 - T_sur)/(R_tot);  %heat flow through circuit
x = q - q_out; %difference between heat flow through circuit and heat
flow out
T5_x = T5_x + .0001;
end

%D is an array of the steady state temperature distribution across the
%assembly
D=zeros(1,in);
D(1,1) = T0;
for i = 2:11
    D(1,i)= D(1,i-1)-q*R_ss/10;
end
for i = 12:single((L_ga/dx+11));
    D(1,i)= D(1,i-1)-q*R_ga/107;
end
for i = single((L_ga/dx + 12)):single((L_ga/dx+21));
    D(1,i)= D(1,i-1)-q*R_ss/10;
end
for i = single((L_ga/dx+22)):in;
    D(1,i)=D(1,i-1)-q*R_al/30;
end

%% Vectors
%"What's your vector, Victor?"

%H vector
H = zeros(1,single(l/dx+11));  %This vector will keep track of the
enthalpy of the PCM in each cell

%k vector
k = zeros(1,single(L/dx+1));
k(1,1:11) = k_hs;
k(1,12:single(l/dx)+11) = k_liquid;
k(1,(single(l/dx)+12):(single(l/dx)+21)) = k_hs;
k(1,(single(l/dx)+22):in) = k_al;

%rho_c solid
rho_c = zeros(1,single(L/dx+1));
rho_c(1,1:11) = rho_hs*c_p_hs;
rho_c(1,12:single(l/dx)+11) = rho_solid*c_p_solid;
rho_c(1,(single(l/dx)+12):(single(l/dx)+21)) = rho_hs*c_p_hs;
rho_c(1,(single(l/dx)+22):in) = rho_al*c_p_al;

%rho_c liquid

%area vector
area = zeros(1,single(L/dx+1));
area(1,1) = .0254*.0508; %heater area
area(1,2:128) = area_h; %heatsink area
area(1,129:in) = area_r; %radiator area

%%
```

```
T = zeros(it,in); %temperature matrix
T(1,:) = D(1,:);
if T0 < T_melt
    H(1,13:end) = 0;
elseif T0 > T_melt
    H(1,13:end) = Hmax;
end

Tm = T(1,:);
for m = 1:(t*60);
    if m <=tt;
        q_in = q_rad;
    else
        q_in = q_stby;
    end
    for n = 1:it-1
        %Surface Node (heater)
        i = 1;
        T(n+1,i) = T(n,i)+(q_in + (k(i)*area(i)*(T(n,i+1)-
T(n,i))/dx))*2*dt/(rho_c(1)*area(i)*dx);
        %Interior Nodes
        for i = 2:12;
            T(n+1,i) = T(n,i) + (k(i-1)*area(i-1)*(T(n,i-1) - T(n,i)) +
k(i)*area(i)*(T(n,i+1) - T(n,i)))*dt/(rho_c(i)*area(i)*dx^2);
        end

        %PCM:
        for i = 13:single(l/dx)+11
            if q_in == q_rad
                if T(n,i) < T_melt && H(i)==0
                    T(n+1,i) = T(n,i) + (k(i-1)*area(i-1)*(T(n,i-1) -
T(n,i)) + k(i)*area(i)*(T(n,i+1) - T(n,i)))*dt/(rho_c(i)*area(i)*dx^2);
                    H(i) = 0;
                    rho_c(i) = rho_solid*c_p_solid;
                end
                if T(n,i) >= T_melt && H(i)==0
                    T(n+1,i) = T_melt;
                    %H(i) = (k(i)*area(i)*(T(n,i+1)-T(n,i-1))/dx)*dt +
H(i);
                    H(i) = (k(i)*area(i)*(T(n,i-1)-T(n,i))/dx +
k(i)*area(i)*(T(n,i+1) - T(n,i))/dx)*dt + H(i);
                    rho_c(i) = rho_liquid*c_p_liquid;
                end
                if T(n,i) == T_melt && H(i)<Hmax && H(i)>0
                    T(n+1,i) = T_melt;
                    %H(i) = (k(i)*area(i)*(T(n,i+1)-T(n,i-1))/dx)*dt +
H(i);
                    H(i) = (k(i)*area(i)*(T(n,i-1)-T(n,i))/dx +
k(i)*area(i)*(T(n,i+1) - T(n,i))/dx)*dt + H(i);
                    rho_c(i) = rho_liquid*c_p_liquid;
                end
                if T(n,i) == T_melt && H(i)>=Hmax
                    T(n+1,i) = T(n,i) + (k(i-1)*area(i-1)*(T(n,i-1) -
T(n,i)) + k(i)*area(i)*(T(n,i+1) - T(n,i)))*dt/(rho_c(i)*area(i)*dx^2);
```

```
                    H(i) = Hmax;
                    rho_c(i) = rho_liquid*c_p_liquid;
                end
                if T(n,i) > T_melt && H(i) == Hmax
                    T(n+1,i) = T(n,i) + (k(i-1)*area(i-1)*(T(n,i-1) -
T(n,i)) + k(i)*area(i)*(T(n,i+1) - T(n,i)))*dt/(rho_c(i)*area(i)*dx^2);
                    H(i) = Hmax;
                    rho_c(i) = rho_liquid*c_p_liquid;
                end

            elseif q_in == q_stby

                if T(n,i) < T_melt && H(i)==0
                    T(n+1,i) = T(n,i) + (k(i-1)*area(i-1)*(T(n,i-1) -
T(n,i)) + k(i)*area(i)*(T(n,i+1) - T(n,i)))*dt/(rho_c(i)*area(i)*dx^2);
                    H(i) = 0;
                    rho_c(i) = rho_solid*c_p_solid;
                end
                if T(n,i) == T_melt && H(i)<=0
                    T(n+1,i) = T(n,i) + (k(i-1)*area(i-1)*(T(n,i-1) -
T(n,i)) + k(i)*area(i)*(T(n,i+1) - T(n,i)))*dt/(rho_c(i)*area(i)*dx^2);
                    H(i) = 0;
                    rho_c(i) = rho_solid*c_p_solid;
                end
                if T(n,i) == T_melt && H(i)>0 %&& H(i)<Hmax
                    T(n+1,i) = T_melt;
                    H(i) = (k(i)*area(i)*(T(n,i+1)-T(n,i-1))/dx)*dt +
H(i);
                    rho_c(i) = rho_liquid*c_p_liquid;
                end
                if T(n,i) <= T_melt && H(i) == Hmax
                    T(n+1,i) = T_melt;
                    H(i) = (k(i)*area(i)*(T(n,i+1)-T(n,i-1))/dx)*dt +
H(i);
                    rho_c(i) = rho_liquid*c_p_liquid;
                end
                if T(n,i) > T_melt && H(i) == Hmax
                    T(n+1,i) = T(n,i) + (k(i-1)*area(i-1)*(T(n,i-1) -
T(n,i)) + k(i)*area(i)*(T(n,i+1) - T(n,i)))*dt/(rho_c(i)*area(i)*dx^2);
                    H(i) = Hmax;
                    rho_c(i) = rho_liquid*c_p_liquid;
                end
            end
        end
        %Interior Nodes
        for i = single(l/dx)+12:in-1;
            T(n+1,i) = T(n,i) + (k(i-1)*area(i-1)*(T(n,i-1) - T(n,i)) +
k(i)*area(i)*(T(n,i+1) - T(n,i)))*dt/(rho_c(i)*area(i)*dx^2);
        end
        %Surface Node (radiator)
        i = in;
        T(n+1,i) = T(n,i) + [epsilon*sigma*area(i)*(T_sur^4 - T(n,i)^4)
+ k(i)*area(i)*(T(n,i-1)-T(n,i))/dx]*dt/(rho_c(i)*area(i)*dx);
    end
```

```
Tn = T(it,1:end);
T(1,1:end) = Tn;
T(2,1:end) = zeros;
Tm = cat(1,Tm,Tn);
end

x1 = linspace(0,t/60,t*60+1);
hs = Tm(:,1);
rr = Tm(:,(l/dx)+23);
fr = Tm(:,in);

plot(x1,hs)
grid on
hold on
%plot(x1,rr)
%plot(x1,fr)
ylim =([270 305]);
xlim =([0 2]);
legend('Heat Sink')
xlabel('Time (Hours)')
ylabel('Kelvin')

csvwrite('IN_Ga_model_full.csv',Tm)

M1 = csvread('1_Met_fullmelt_vacglz_MLI.csv');
M1(:,1) = (M1(:,1)/3600);
M1(:,2:5) = M1(:,2:5)+273;
hold on
plot(M1(1:1081,1),M1(1:1081,2))
xlim = ([0 3]);
line([.519 .519],[270 310],'Color','r')

%Why is this gallium still liquid below its melting point?  Because
it's so cool, it's supercool.
```

Code for Lumped Capacitance Model

```
%simple model, vacuum, max temp limit and cool

clear all, close all, clc

T0 = 273; %Kelvin
T_min = 267; %Kelvin, room temp
T_sur = 265; %Kelvin
T_max = 308; %Kelvin
q = 10; %watts
dt = 1; %second
T_melt = 302; %Kelvin
epsilon = .86;
sigma = 5.67E-8;
area_r = .01; %meters
mass_Ga = 0.093; %kg
mass_tot = .26666; %kg, mass of test article
c_p_Ga = 370.9; %J/kg-K, Ga specific heat
c_p_tot = 613.3; %J/kg-K, average specific heat for test article
Hmax = mass_Ga*80170; %Joules, max latent heat
T(1,2:4) = zeros;

q_in = q;
T(1,1) = 0;
T(1,2) = T0;
T(1,3) = (q_in - (epsilon*sigma*area_r*(T(1,2)^4 -
T_sur^4)))/(mass_Ga*c_p_tot);
if T(1,2)>T_melt
    T(1,4)=Hmax;
end

i=2;
while T(i-1,2)<T_max
    if T(i-1,2)<=T_melt && T(i-1,4)<=0
        T(i,2) = T(i-1,3)*dt+T(i-1,2);
        T(i,3) = (q_in - (epsilon*sigma*area_r*(T(i,2)^4 -
T_sur^4)))/(mass_tot*c_p_tot);
        T(i,4) = 0;
    end
    if T(i-1,2)>=T_melt && T(i-1,4)<=Hmax
        T(i,2) = T_melt;
        T(i,3) = (q_in - (epsilon*sigma*area_r*(T(i,2)^4 -
T_sur^4)))/(mass_tot*c_p_tot);
        T(i,4) = (q_in - (epsilon*sigma*area_r*(T(i-1,2)^4 -
T_sur^4)))*dt + T(i-1,4); %enthalpy tracker
    end
    if T(i-1,2)>=T_melt && T(i-1,4)>=Hmax
        T(i,2) = T(i-1,3)*dt+T(i-1,2);
        T(i,3) = (q_in - (epsilon*sigma*area_r*(T(i,2)^4 -
T_sur^4)))/(mass_tot*c_p_tot);
        T(i,4) = Hmax;
    end
```

```
    T(i,1)=T(i-1,1)+dt;
    i=i+1;
end

q_in = 0;
while T(i-1,2)>T_min+.001
    if T(i-1,2)<=T_melt && T(i-1,4)<=0
        T(i,2) = T(i-1,3)*dt+T(i-1,2);
        T(i,3) = (q_in - (epsilon*sigma*area_r*(T(i,2)^4 -
T_sur^4)))/(mass_tot*c_p_tot);
        T(i,4) = 0;
    end
    if T(i-1,2)<=T_min
        T(i,2) = T_min;
        T(i,3) = (q_in - (epsilon*sigma*area_r*(T(i,2)^4 -
T_sur^4)))/(mass_tot*c_p_tot);
        T(i,4) = 0;
    end
    if T(i-1,2)>=T_melt && T(i-1,4)<=Hmax && T(i-1,4)>0
        T(i,2) = T_melt;
        T(i,3) = (q_in - (epsilon*sigma*area_r*(T(i,2)^4 -
T_sur^4)))/(mass_tot*c_p_tot);
        T(i,4) = (q_in - (epsilon*sigma*area_r*(T(i,2)^4 -
T_sur^4)))*dt+T(i-1,4);
    elseif T(i-1,2)<=T_melt && T(i-1,4)<=Hmax && T(i-1,4)>0
        T(i,2) = T_melt;
        T(i,3) = (q_in - (epsilon*sigma*area_r*(T(i,2)^4 -
T_sur^4)))/(mass_tot*c_p_tot);
        T(i,4) = (q_in - (epsilon*sigma*area_r*(T(i,2)^4 -
T_sur^4)))*dt+T(i-1,4);
    end
    if T(i-1,2)>=T_melt && T(i-1,4)>=Hmax
        T(i,2) = T(i-1,3)*dt+T(i-1,2);
        T(i,3) = (q_in - (epsilon*sigma*area_r*(T(i,2)^4 -
T_sur^4)))/(mass_tot*c_p_tot);
        T(i,4) = Hmax;
    end
    T(i,1)=T(i-1,1)+dt;
    i=i+1;
end

%plots
x1 = T(1:10:end,1)/3600;
y1 = T(1:10:end,2);
plot(x1,y1)
```

Appendix B: Month-Long Orbit Simulation Results

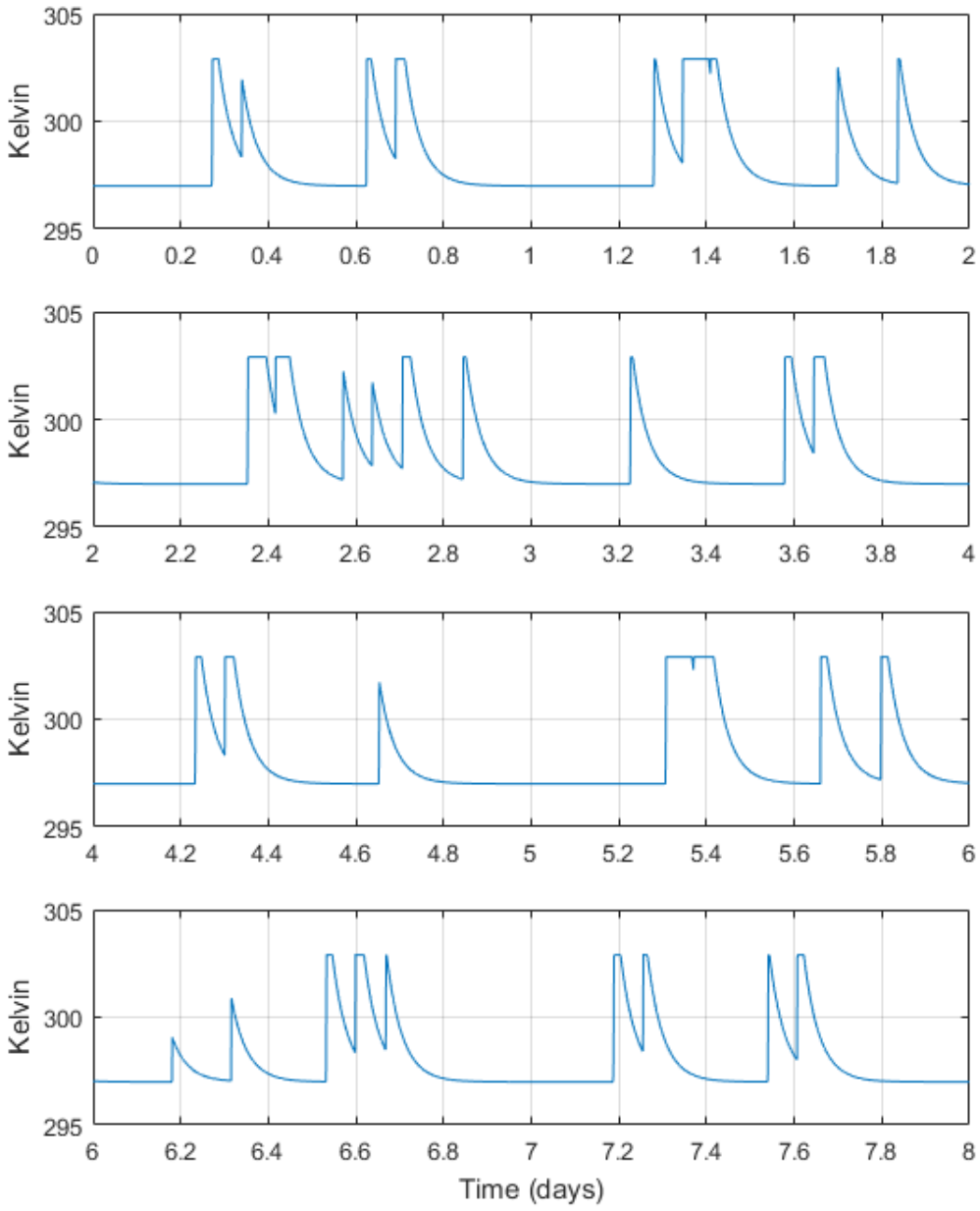

Figure 30 Orbit Simulation: Day 0 - 8

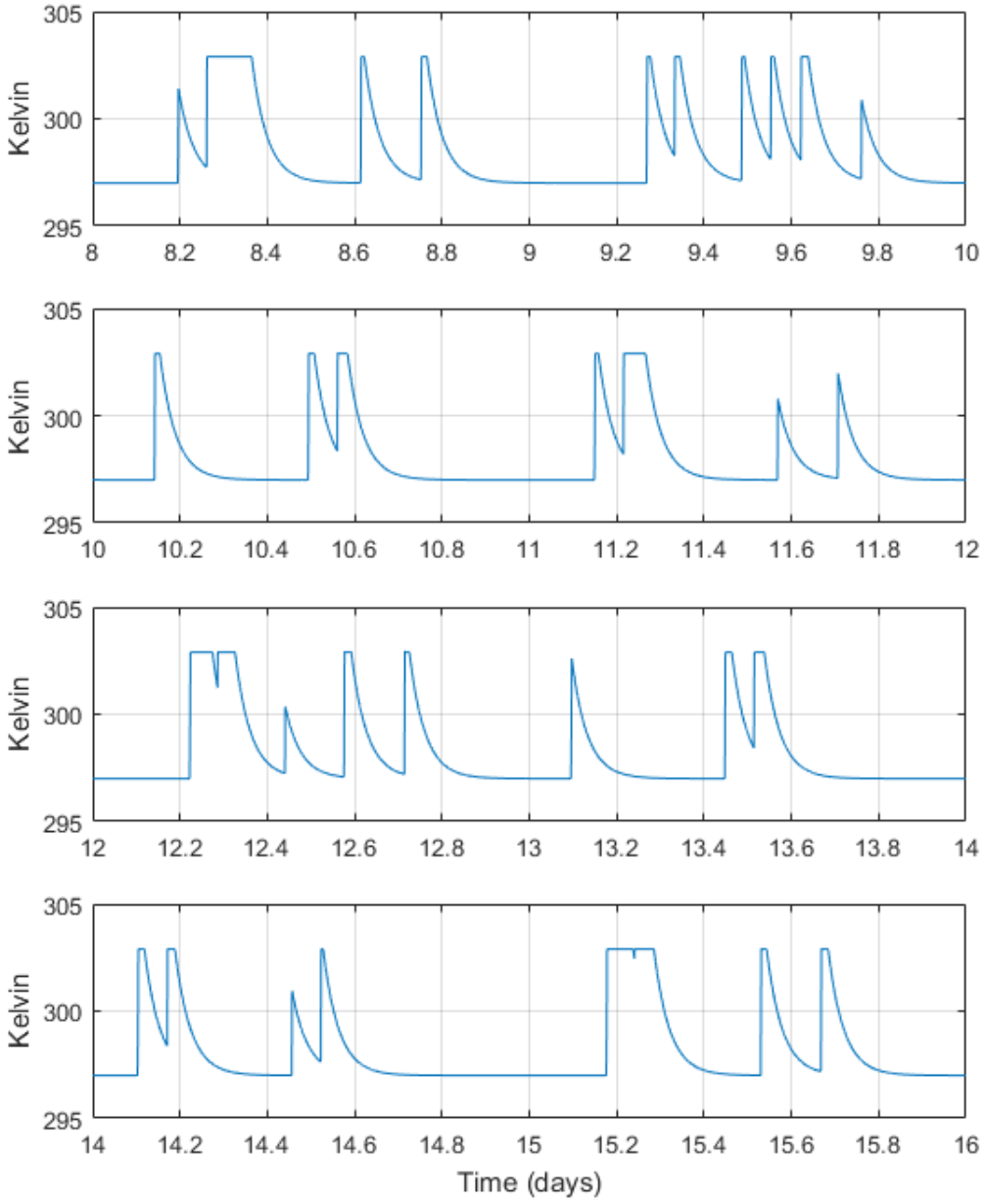

Figure 31 Orbit Simulation: Day 8 - 16

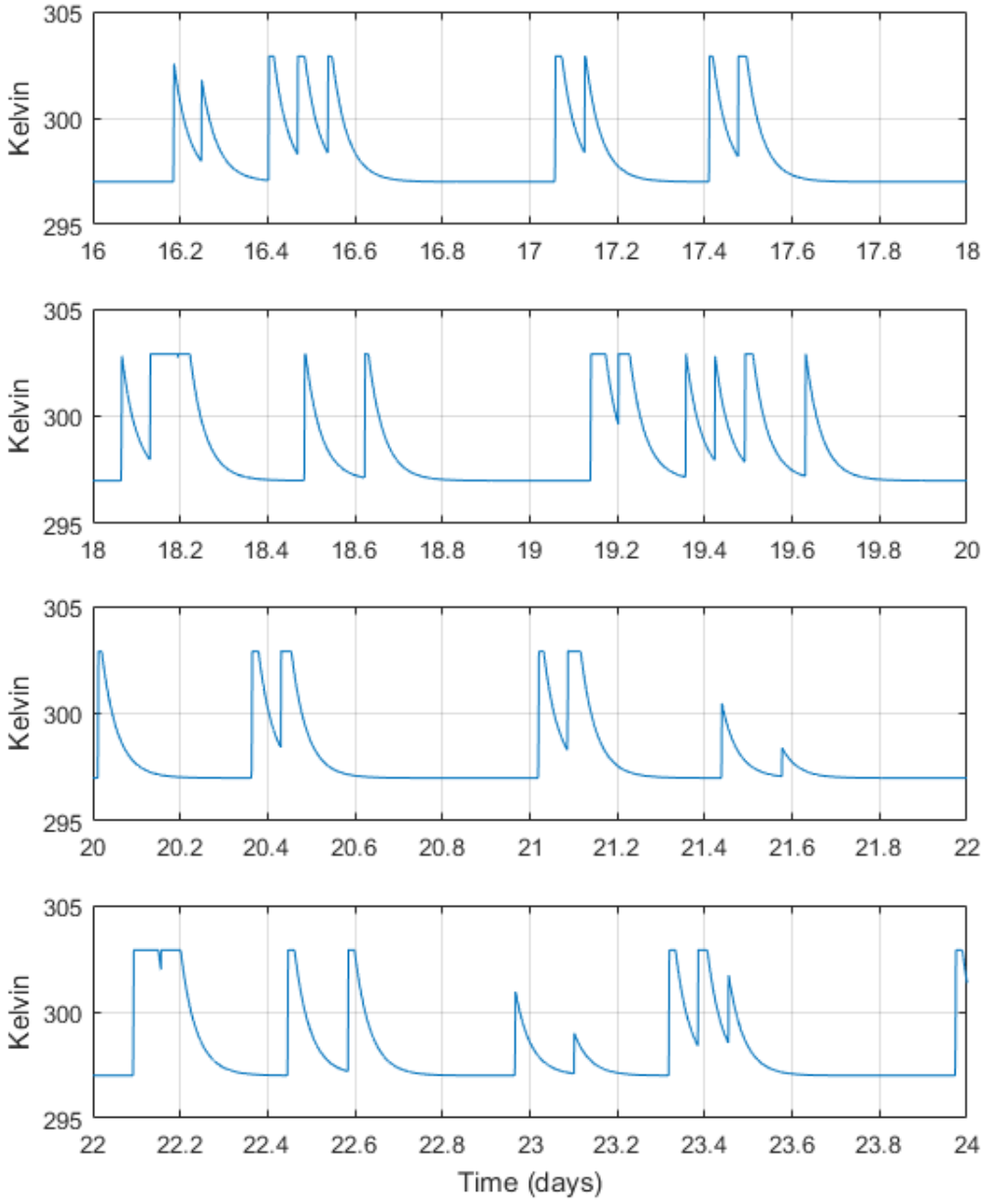

Figure 32 Orbit Simulation: Day 16 - 24

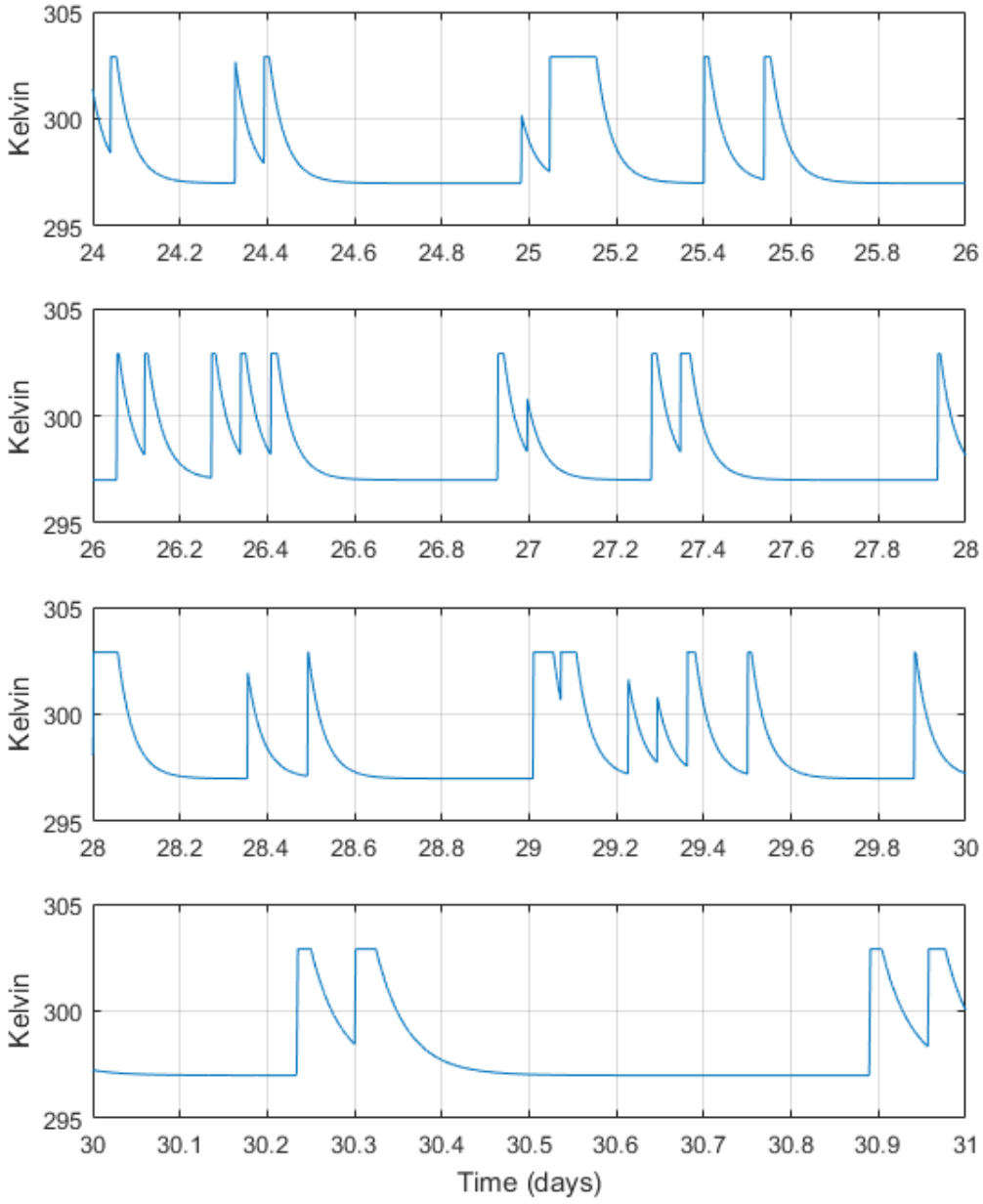

Figure 33 Orbit Simulation: Day 24 – 31

Appendix C: Equipment and Materials Used

Thermal vacuum chamber
K-type thermocouples (Minco™ TC40KT40A)
Polyimide Thermofoil™ Heaters (Minco™ HK6907)
DC power supply
Thermally conductive epoxy (3M™ TC-2810)
Kapton tape
Multimeter
Thermal Insulators (ULTEM 9085)
Gallium Heat sinks (Inconel 718, Stainless Steel 316, ULTEM 9085)
Flat plate radiators (100 mm x 100 mm x 3.2 mm)
Aeroglaze® Z276
Hot plate
Beakers
Thread seal tape
Thermometer
Pipe plugs (1/16” and 3/8”)

Bibliography

[1] P. K. Schelling, L. Shi and K. E. Goodson, "Managing Heat for Electronics," *Materials Today,* vol. 8, no. 6, pp. 30-35, 2005.

[2] G. Quinn, E. Hodgson and R. Stephan, "Phase Change Material Trade Study: a Comparison between Wax and Water for Manned Spacecraft," in *American Institute of Aeronautics and Astronautics*, Portland, OR, 2011.

[3] P. Luebbers and O. Chopra, "Compatibility of ITER Candidate Materials with Static Gallium," in *IEEE/NPSS Symposium Fusion Engineering*, 1995.

[4] "Encyclopaedia Britannica," 12 October 2016. [Online]. Available: https://www.britannica.com/science/latent-heat. [Accessed 11 December 2017].

[5] T. L. Bergman, A. S. Lavine, F. P. Incropera and D. P. Dewitt, Fundamentals of Heat and Mass Transfer, 7th ed., John Wiley & Sons, 2011.

[6] S. Z. Fixler, "Satellite Thermal Control Using Phase-Change Materials," *Journal of Spacecraft and Rockets,* vol. 3, no. 9, pp. 1362-1368, 1966.

[7] M.-H. Chen, J.-D. Huang and C.-R. Chen, "An Investigation on Phase Change Device for Satellite Thermal Control," in *7th International Conference on Mechanical and Aerospace Engineering*, London, 2016.

[8] D. V. Hale, M. J. Hoover and M. J. O'Neill, "Phase Change Materials Handbook," Lockheed Missiles and Space Company, Huntsville, 1971.

[9] R. Sheth, "NASA," 19 July 2017. [Online]. Available: https://www.nasa.gov/mission_pages/station/research/experiments/2077.html. [Accessed 6 August 2017].

[10 I. S. Edward Hawkins, S. L. Murchie, K. J. Becker, C. M. Selby, F. S. Turner, M. W. Noble, N. L. Chabot, T. H. Choo, E. H. Darlington, B. W. Denevi, D. L. Domingue, C. M. Ernst, G. M. Holsclaw, N. R. Laslo, W. E. McClintock, L. M. Prockter, M. S. Robinson, S. C. Solomon and I. R. E. Sterner, "In-Flight

Performance of MESSENGER's Mercury Dual Imaging System," in *Instruments and Methods for Astrobiology and Planetary Missions* , 2009.

[11 S. Mondal, "Phase Change Materials for Smart Textiles - An overview," *Applied Thermal Engineering,* vol. 28, no. 11-12, pp. 1536-1550, 2008.

[12 B. Zalba, J. M. Marin, L. F. Cabeza and H. Mehling, "Review on thermal energy storage with phase change: materials, heat transfer analysis and applications," *Applied Thermal Engineering,* vol. 23, no. 3, pp. 251-283, 2003.

[13 "pcmproducts.net," Phase Change Material Products Limited, [Online]. Available: http://www.pcmproducts.net/files/plusice_range2011.pdf. [Accessed 2 May 2018].

[14 S. K. Saha, K. Srinivasan and P. Dutta, "Studies on Optimum Distribution of Fins in Heat Sinks Filled with Phase Change Materials".

[15 H. Ge, H. Li, S. Mei and J. Liu, "Low melting point liquid metal as a new class of phase change material: An emerging frontier in energy area," *Renewable and Sustainable Energy Reviews,* vol. 21, pp. 331-346, 2013.

[16 H. Ge and J. Liu, "Keeping Smartphones Cool with Gallium Phase Change Material," *ASME. Journal of Heat Transfer,* vol. 135, no. 5, 2013.

[17 "Additivemanufacturing.com," AMazing, 2017. [Online]. Available: http://additivemanufacturing.com/basics/. [Accessed 29 August 2017].

[18 I. Gibson, D. Rosen and B. Stucker, Additive Manufacturing Technologies 3D Printing, Rapid Protyping, and Direct Digital Manufacturing, Second Edition, New York: Springer, 2015.

[19 E. W. Frazier, "Metal Additive Manufacturing: A Review," *Journal of Materials Engineering and Performance,* vol. 23, no. 6, pp. 1917-1928, 2014.

[20 J. C. Tannehill, D. A. Anderson and R. H. Pletcher, Computational Fluid Mechanics and Heat Transfer, 2nd Edition, Washington, D.C.: Taylor & Francis, 1997.

[21 Astronautical Development, LLC., "AstroDev.com," 1 September 2009. [Online]. Available: http://www.astrodev.com/public_html2/downloads/datasheet/LithiumUserManual.pdf. [Accessed 11 December 2017].

[22 J. E. Oberright, "Spacecraft Thermal Control," in *Space Mission Engineering: The New SMAD*, Hawthorne, Microcosm Press, 2011, pp. 685-700.

[23 I. Minco Products, "catalog.minco.com," 2018. [Online]. Available: http://catalog.minco.com/catalog3/d/minco/?c=products&cid=3_1-polyimide-thermofoil-heaters&id=HK6907. [Accessed 8 November 2018].

[24 I. Minco Products, "www.minco.com," 2018. [Online]. Available: https://www.minco.com/ResourceCenter/FAQs/Heaters. [Accessed 8 November 2018].

[25 Minco Products, Inc., "www.minco.com," 2018. [Online]. Available: https://www.minco.com/~/media/files/minco/productguides/heat/heater%20design%20guide.ashx. [Accessed 8 November 2018].

[26 T. Articles, "Allboutcircuits.com," EETech Media, LLC, 2018. [Online]. Available: https://www.allaboutcircuits.com/textbook/direct-current/chpt-12/temperature-coefficient-resistance/. [Accessed 28 Nov 2018].

REPORT DOCUMENTATION PAGE

Form Approved
OMB No. 074-0188

1. REPORT DATE *(DD-MM-YYYY)*	**2. REPORT TYPE**	**3. DATES COVERED** *(From – To)*
13-12-2018	Master's Thesis	September 2016 – December 2018

TITLE AND SUBTITLE

Thermal Management of Satellite Electronics via Gallium Phase Change Heat Sink Devices

5a. CONTRACT NUMBER

5b. GRANT NUMBER

5c. PROGRAM ELEMENT NUMBER

6. AUTHOR(S)

Palmer, Brian O., Major, USAF

5d. PROJECT NUMBER

5e. TASK NUMBER

5f. WORK UNIT NUMBER

7. PERFORMING ORGANIZATION NAMES(S) AND ADDRESS(S)
Air Force Institute of Technology
Graduate School of Engineering and Management (AFIT/ENY)
2950 Hobson Way
Wright-Patterson AFB OH 45433-7765

8. PERFORMING ORGANIZATION REPORT NUMBER

AFIT-ENY-MS-18-D-038

9. SPONSORING/MONITORING AGENCY NAME(S) AND ADDRESS(ES)

Intentionally left blank

10. SPONSOR/MONITOR'S ACRONYM(S)

11. SPONSOR/MONITOR'S REPORT NUMBER(S)

12. DISTRIBUTION/AVAILABILITY STATEMENT
DISTRUBTION STATEMENT A. Approved For Public Release; Distribution Unlimited.

13. SUPPLEMENTARY NOTES
This material is declared a work of the U.S. Government and is not subject to copyright protection in the United States.

14. ABSTRACT

The purpose of this research was to determine the effectiveness and feasibility of additively manufactured heat sinks using gallium as a phase change material in the thermal management of satellite electronics. A design was created based on the footprint of an Astronautical Development, LLC Lithium 1 UHF radio and six heat sinks were additively manufactured; two each of stainless steel 316, Inconel 718, and ULTEM 9085. Each heat sink was filled with gallium for testing purposes. Models were created to simulate the behavior of the heat transfer and phase change processes occurring within the heat sink. Additionally, laboratory data was gathered on the actual processes occurring. Testing was carried out in a thermal vacuum chamber with the use of film heaters that were attached to the heat sinks to simulate radios in transmitting mode while a satellite is in contact with a ground station. Finally, temperature profiles of the laboratory data were created to gain insight into the characteristics of the phase change process and its effectiveness in thermal management of satellite electronics.

15. SUBJECT TERMS
Passive Thermal Management, Additive Manufacturing, Phase Change Material, Gallium, Heat Sink

16. SECURITY CLASSIFICATION OF:			**17. LIMITATION OF ABSTRACT**	**18. NUMBER OF PAGES**	**19a. NAME OF RESPONSIBLE PERSON**
a. REPORT	**b. ABSTRACT**	**c. THIS PAGE**			Dr. Carl R. Hartsfield, AFIT/ENY
U	**U**	**U**	**UU**	102	**19b. TELEPHONE NUMBER** *(Include area code)* (937) 255-3636, ext 4667 (brian.palmer.9@us.af.mil)

Standard Form 298 (Rev. 8-98)
Prescribed by ANSI Std. Z39-18